Lateral Strength Evaluation of Ferrocement Strengthened Masonry Infilled RC frame Based on Experimentally Observed Failure Mechanisms

Debasish Sen (debasish.ce@aust.edu)
Ahsanullah University of Science and Technology https://orcid.org/0000-0001-6375-4596
Hamood Alwashali
Tohoku University: Tohoku Daigaku
Md Shafiul Islam
Tohoku University: Tohoku Daigaku
Matsutaro Seki
Building Research Institute
Masaki Maeda
Tohoku University: Tohoku Daigaku

Research Article

Keywords: Ferrocement, Infill masonry, Strengthening, Failure mechanism, Capacity evaluation

Posted Date: April 27th, 2021

DOI: https://doi.org/10.21203/rs.3.rs-422754/v1

Lateral Strength Evaluation of Ferrocement Strengthened Masonry Infilled RC frame Based on Experimentally Observed Failure Mechanisms

Debasish Sen[*]**,** Assistant Professor, Department of Civil Engineering, Ahsanullah University of Science and Technology, Dhaka, Bangladesh, debasish.ce@aust.edu

Hamood Alwashali, Assistant Professor, Graduate School of Engineering, Department of Architecture and Building Science, Tohoku University, Sendai, Japan, hamood@rcl.archi.tohoku.ac.jp

Md Shafiul Islam, Assistant Professor, Graduate School of Engineering, Department of Architecture and Building Science, Tohoku University, Sendai, Japan, shafiul@rcl.archi.tohoku.ac.jp

Matsutaro Seki, Research Fellow, Building Research Institute, Tsukuba, Japan, sekimatsutaro@yahoo.co.jp

Masaki Maeda, Professor, Graduate School of Engineering, Department of Architecture and Building Science, Tohoku University, Sendai, Japan, maeda@rcl.archi.tohoku.ac.jp

Abstract

In developing countries, lateral strengthening of seismically vulnerable masonry infilled RC buildings is one of the major concern. In this context, ferrocement can be used as a low cost and less labor-intensive strengthening scheme for those buildings. This study aims to experimentally identify major failure mechanisms, and to develop a lateral strength evaluation procedure of ferrocement strengthened masonry infilled RC frame. Subsequently, ductility of all of the identified major failure mechanisms is compared. Mainly four major failure mechanisms (i.e. overall flexural, column punching-joint sliding, diagonal compression, and diagonal cracking-sliding) are identified from the current experimental work and past experimental studies. The strength evaluation procedure, based on the identified failure mechanisms, is proposed and verified with an average calculated to experimental lateral strength ratio of 0.8. Among the identified failure mechanisms, overall flexural, and diagonal cracking-sliding mechanisms showed relatively ductile behavior when compared to the ductility of column punching-joint sliding, and diagonal compression failure mechanism.

Keywords: Ferrocement; Infill masonry; Strengthening; Failure mechanism; Capacity evaluation

Declaration

Funding: JICA, Japan under SATREPS-TSUIB project (https://www.satreps-tsuib.net/)
Conflicts of interest/Competing interests: N/A

Acknowledgement

This research is supported and funded by JICA under SATREPS–TSUIB project (principle investigators: Prof. Yoshiaki Nakano, U. Tokyo and Mr. Md Ashraful Alam, HBRI, Bangladesh). The experimental work has been conducted in Maeda Laboratory, Tohoku University, Japan as a part of PhD research of the first author. Hence authors extend their thanks to all of the students of the laboratory, especially Mr. Yuta Torihata and Ms. Zasiah Tafheem for their cordial help in the experimental work. A special thanks to Prof. Dr. Sharmin Reza Chowdhury, AUST for his cordial cooperation in the research project.

---

[*] Corresponding author

1 Introduction

In developing countries, seismic strengthening of existing buildings is one of the most important concerns for structural engineers because there are many seismically vulnerable buildings. Lateral capacity improvement of these existing vulnerable buildings could be conducted by insertion of additional structural elements e.g. shear wall, steel bracing, etc. or by increasing the lateral capacity of existing elements i.e. jacketing of RC columns, beams, walls, etc. Structural element insertion would be difficult to apply in several thousands of existing RC buildings of developing countries due to limitation of expertise and capital. On the other hand, jacketing technology might be a feasible approach for developing countries, if it could be conducted with less technical efforts and capital. In many developing countries, the common structural system of buildings is RC moment resisting frame with non-structural masonry infill walls which might be a probable candidate for strengthening. Some reinforcing material is required to convert the existing infill masonry to structural components with an intension to attain a reliable performance during an earthquake. The approach of converting infill masonry to structural components might serve two purposes. First, it would be a strengthening method and second, it might prevent the un-expected low strength of masonry infilled RC frame caused by short column effect by sliding of infill masonry. Strengthening of existing infill masonry can be conducted by Ferrocement (FC) lamination, Textile mortar reinforcement (TRM), Fiber reinforced mortar (FRM), etc. Among these, ferrocement lamination is a low cost and less labor intensive strengthening method for developing countries. As a part of SATREPS-TSUIB project in Bangladesh (https://www.satreps-tsuib.net/), which is sponsored by JICA (Japan International Cooperation Agency), authors are trying to develop an effective evaluation procedure of ferrocement strengthened masonry infilled RC frame.

Ferrocement strengthening of masonry refers to the application of an initial mortar layer on both surfaces of the masonry wall which is followed by the placement of steel mesh reinforcement and a second mortar layer, as shown in Fig. 1. Anchorages are also being used to attach wire-mesh to masonry and RC frame. Hereafter, the term “Ferrocement” will be stated as “FC” throughout the article. Though FC has been studied for decades as a construction material, there is no design specification e.g. amount of mesh reinforcement, mortar thickness, etc. for use as a shear strengthening material on unreinforced infilled masonry. The paucity of comprehensive studies on FC strengthening has also been acknowledged in ACI 549 (1997). Though, several researchers (Kaya et al. 2018, Seki et al. 2018, Demirel et al. 2015, Altin et al. 2010, Zarnic and Tomazevic 1985) studied the effect of FC on the lateral behavior of masonry infilled RC frame, however, the main intention was to improve seismic capacity rather than to identify and evaluate experimentally observed failure mechanisms.

Therefore, this study initially aims to recognize major failure mechanisms of masonry infilled RC frame with ferrocement strengthening based on a new experimental campaign (with 2 half-scaled specimens) as well as from past experimental studies. Then, endeavor is taken to propose and validate

lateral strength evaluation of the FC strengthened masonry infilled RC frame based on the recognized major failure mechanisms. Finally, experimental ductility level of the major failure mechanisms is compared.

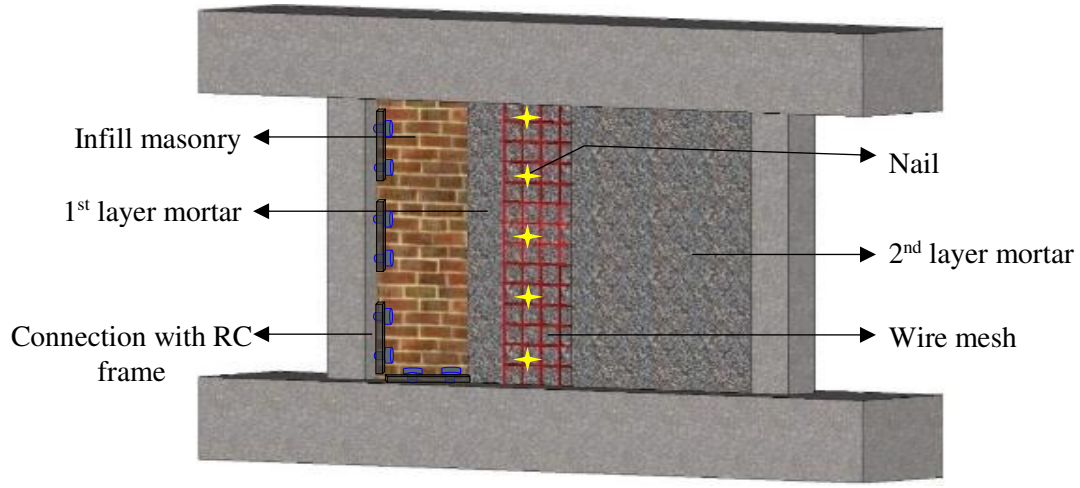

Fig. 1 Schematic diagram of FC strengthened masonry infill

2 Identified load transfer mechanisms in past experimental studies

In general, seismic performance evaluation of a structural component needs a proper understanding of load transfer mechanism i.e. failure mechanism of that structural component. Therefore, an attempt is taken here to understand load transfer mechanisms of masonry infilled RC frame after ferrocement strengthening. Since ferrocement is to be used for strengthening of masonry infilled RC frame, it is also necessary to understand the failure mechanisms of un-strengthened masonry infilled RC frame prior. It will help to anticipate the most probable failure mechanisms of masonry infilled RC frame after ferrocement strengthening.

Generally, the failure mechanism of masonry infilled RC frame depends on relative stiffness as well as the strength of infill material compared to the surrounding RC frame (ASCE/SEI 41-06 2001). At lower lateral displacement, masonry infilled RC frame works similar to a monolithic infilled frame. Then, with the increasing lateral displacement, a separation occurs between frame and infill masonry, subsequently, the RC frame acts like a braced RC frame. Before separation, the infilled RC frame can also fail by overturning or rocking like a flexural wall when the infill masonry is very strong and stiff. Overall flexural failure (i.e. rocking) can happen when the RC column is lightly reinforced (FEMA 306 1998) and this failure has been reported in a study by Adnan et al. (2019). After separation of masonry and the surrounding frame, if the infilled RC frame can escape overall flexural failure, the lateral load is carried by both components therefore both RC frame and masonry experience damages. In general infill masonry exhibits diagonal compression crushing, joint sliding, and/ or diagonal cracking, whereas RC columns fail by the formation of plastic hinges or shear failure of RC columns. In some of the cases, especially when sliding occurs at the mid-height, a short column is also evident (Zahura et al. 2020 and Alwashali et al. 2018). By careful observation, it has been perceived that diagonal cracking of infill

masonry precedes sliding of un-strengthened masonry infill masonry, as observed in the experimental work by authors in Zahura et al. (2020) and Alwashali et al. (2018), therefore the combination of sliding and diagonal cracking is considered herein as one of the failure mechanism. However, when the sliding plane is at the interface of beam soffit and upper infill masonry course, it might also be possible to get an extremely short column failure of the tension column that might fail by horizontal slip shear failure, as shown in Fig. 2, reported by Crisafulli 1997. This almost horizontal slip failure of the column is recognized by JBDPA (2001) especially for concrete infilled RC frame and generally known as punching shear failure of the column. Therefore, this extremely short column failure of the RC column is cited, hereafter, as punching shear failure. In brief, four failure mechanisms, i.e. overall flexural failure, column punching-joint sliding, diagonal compression, and sliding - diagonal cracking, are expected for un-strengthened masonry infilled RC frame (Sen 2020).

However, such categorization of failure mechanisms for ferrocement strengthened masonry infilled RC frame is not documented well. Therefore, a careful literature survey has been conducted from past experimental studies on FC strengthened test specimens (Kaya et al. 2018, Seki et al. 2018, Demirel et al. 2015, Altin et al. 2010, Zarnic and Tomazevic 1985) in order to understand the major load transfer mechanisms i.e. failure mechanisms of ferrocement strengthened masonry infilled RC frame. In those studies (Kaya et al. 2018, Seki et al. 2018, Demirel et al. 2015, Altin et al. 2010, Zarnic and Tomazevic 1985), both solid clay bricks and hollow bricks, having masonry compressive strength of 5 ~ 15MPa, were used to build infill masonry. The masonry infills were strengthened using ferrocement having a mortar strength of 3 ~ 30MPa and wire mesh ratio of 0.05 ~ 0.35%.

Kaya et al. (2018) conducted an experimental investigation having seven FC strengthened infill hollow brick masonry specimens. The main variables were the embedment length and spacing of the dowel bar, where dowel bars have been used to transfer shear from the RC frame to the FC layer. It is to be noted that FC has been applied on one side of the infill panel only. The strengthened surface experienced a distributed shear cracks pattern and the failure mechanism has been recognized as diagonal compression mechanism. The experimental investigation indicated that the dowel length and spacing did not affect the maximum resistance which is on average 1.5 times when compared to the un-strengthened masonry infilled RC frame.

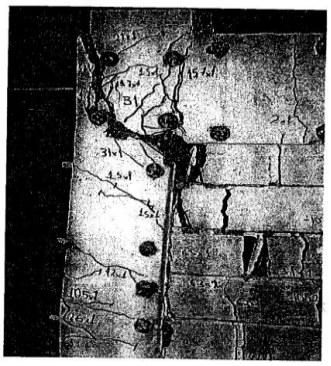

Fig. 2 Extremely short column i.e. punching failure of tension column (Crisafulli 1997)

Table 1: Ferrocement strengthened test specimens in past studies

Reference	Specimen	Maximum resistance, Q_{exp} (kN)	Observed failure mechanism	Strength improvement
Kaya et al. (2018)	Sp-3	140	Diagonal compression	1.40 ~1.60
	Sp-4	150		
	Sp-5	155		
	Sp-6	140		
	Sp-7	145		
	Sp-8	145		
	Sp-9	135		
	Sp-10	135	*Delamination	-
	Sp-11	145		
Seki et al. (2018)	S5-FMFC	330	Diagonal cracking-sliding	1.70
Demirel et al. (2015)	SMF	181	Diagonal compression	1.50
Altin et al. (2010)	Sp-2	110	*Sliding at dowel tip	-
	Sp-3	155	**Crushed at grid of mesh reinforcement	-
	Sp-4	191	Diagonal cracking	2.50
Zarnic and Tomazevic (1985)	M3	333	Diagonal cracking	1.03
	M4	389	**Diagonal cracking	1.20

* Identified as premature failure ** Reinforcement was inserted to RC frame, not usual

Seki et al. (2018) investigated several retrofit or strengthening schemes for brick masonry infilled RC frame system where one test specimen has been strengthened with FC lamination. Initially, the strengthened infill masonry started to act like a structural wall with distributed diagonal cracks, and finally, it slid horizontally and pushed the tension column to fail in shear at top. FC lamination improved the lateral strength at about 1.7 times, as reported in Table 1, with a reduced ductility i.e. peak story drift.

Demirel et al. (2015) also investigated the lateral behavior of FC strengthened masonry infilled RC frame and observed that the applied strengthening method improved lateral strength about 1.5 times when compared to masonry infilled RC frame. The strengthened infill panel was crushed at the corner, which is very common for hollow block masonry, which leads to converging the lateral behavior like bare RC frame at the post-peak stage. Even at large story drift, the strengthened infill masonry remained intact except the aforementioned crushing at the loading corner.

Altin et al. (2010) studied FC laminated masonry infilled RC frames; including two specimens with varying mortar strength. The experimental observation demonstrated that the specimen with higher FC mortar strength (30MPa) leads to higher lateral resistance i.e. 1.7 times when compared to the specimen with lower FC mortar strength (5MPa). The failure mechanism of the specimen with higher FC mortar strength (30MPa) has been recognized as diagonal cracking, whereas specimens with and

lower FC mortar strength exhibited bearing failure of mortar at dowel bar tips. In another strengthened specimen, instead of dowel bar insertion, the mesh reinforcement has been inserted in the surrounding RC frame. It improved the lateral strength about two times when compared to the un-strengthened specimen while strength improvement with dowel connection was about 1.4 times. This observation reflects the much importance of the connection of mesh reinforcement to the surrounding RC frame rather than the connection of mortar to the RC frame. It is worthy to note that sometimes delamination was also happened (Kaya et al. 2018), however delamination is not considered as a major failure mechanism i.e. load transfer mechanism.

In past studies, mainly two major load transfer mechanisms i.e. diagonal compression (Kaya et al. 2018 and Demirel et al. 2015), and diagonal cracking-sliding (Seki et al. 2018, Altin et al. 2010, Zarnic and Tomazevic 1985) were evident where both FC strengthened infill panel and surrounding RC frame damaged simultaneously. This could be attributed to the low strength masonry as well as FC mortar. If infill masonry and strengthening mortar had higher strength it could have more impact on the surrounding frame with concentrated damage of the surrounding RC frame only like an overall flexural failure, and column punching-joint sliding failure that have been found for un-strengthened masonry infilled RC frame. Since, overall flexural failure, and column punching-joint sliding failure are not evident in past studies, therefore it is necessary to investigate ferrocement strengthening on strong masonry infill i.e. high compressive strength. This is the main motivation for the experimental investigation on ferrocement strengthening of strong masonry infilled RC frame which is discussed in the following section. At the same time, past experimental studies focused on the mortar strength and connection of FC with the RC frame as governing parameters of FC strengthened masonry infilled RC frame. However, the amount of wire mesh has not been studied yet, therefore wire mesh ratio is set as the variable for test specimens.

3 Experimental program

3.1 Specimen design concept

Two half-scaled ferrocement strengthened masonry infilled RC frames, as shown in Fig. 3(a)-(d), are designed to be in line with the objective of this study. The design aspect of each component is discussed below:

RC frame

As mentioned earlier, this study is focused to be applied in Bangladesh therefore a cross-section of 200 x 200mm of the RC column has been adopted as a half scaled dimension to represent field practice in Bangladesh. The long and shear reinforcements of the RC columns have been designed as a flexural column. The top beam was intentionally kept very stiff to avoid failure on the beam.

Infill masonry

Strong masonry infill (masonry compressive strength > 25MPa) was built inside the RC frame for

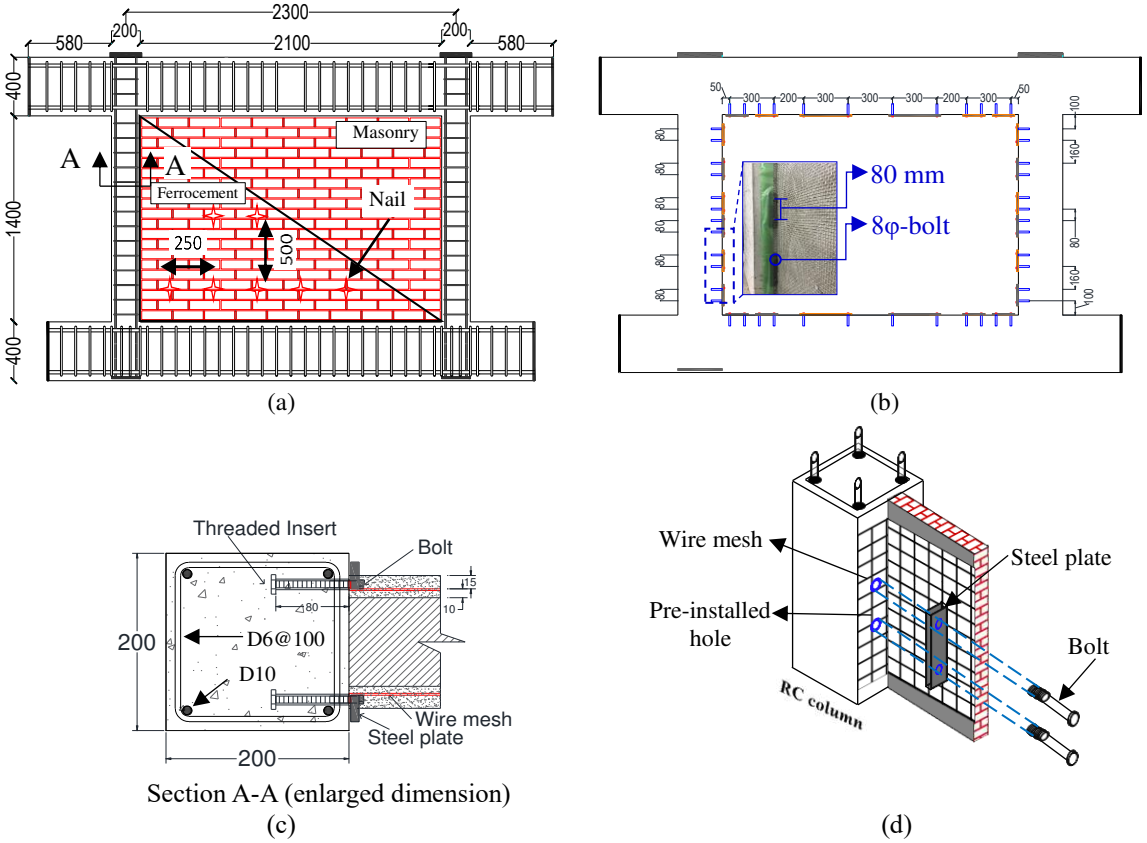

Fig. 3 (a) geometry of test specimen (dimension in mm) (b) locations of drilled holes in RC frame and (c) cross section of column and (d) connection method of wire mesh with RC frame (both columns and beams)

strengthening purpose and to understand the effect of strong FC strengthened infill panel on the surrounding RC frame's failure.

Ferrocement

Several types (i.e. square, hexagonal, diamond shape) of mesh reinforcements are available which can be used for FC strengthening of masonry. In this study, steel wire mesh having square spacing is adopted for infill masonry strengthening because square wire mesh is recommended by ACI 549R (1997) to use where the biaxial stress field is prominent e.g. masonry infill. In this study, wire mesh content is selected based on past literature survey, since there is no design guideline for ferrocement strengthening of masonry infilled RC frame. In past studies (Kaya et al. 2018, Seki et al. 2018, Demirel et al. 2015, Altin et al. 2010, Zarnic and Tomazevic 1985), horizontal mesh reinforcement was kept within a range of 0.05~0.35% of the horizontal masonry area. Since the objective of this experimental program is to investigate the impact of infill panel on the surrounding RC frame, therefore wire mesh ratio for the current study has been set to 0.16% (relatively low ratio) for specimen IM-FC-1 and 0.56% (relatively high ratio) for specimen IM-FC-2. For specimen IM-FC-2, wire mesh ratio has been set almost 3.5 times than specimen IM-FC-1, to investigate the effect of higher wire mesh ratio on the failure mechanism of the surrounding RC frame.

Connection with RC frame and masonry

In general, the connection of FC layer with the RC frame can be established by dowel bars. However, Kaya et al. (2018) concluded that dowel spacing and dowel embedment length might not have an influence on the lateral strength of FC strengthened masonry infilled RC frame. In addition, Altin et al. (2010) found that the dowel bar causes premature bearing failure of the FC mortar layer without much improvement in lateral capacity in case of low strength mortar which is commonly used in developing countries. One additional point to be noted that very stiff connection, i.e. dowel bar, between mortar and RC frame might cause easy splitting of the applied FC mortar layer in case of low strength mortar since no spiral reinforcement is provided. Therefore, the dowel connection is not considered herein. The insertion of mesh reinforcement in the RC frame is effective than dowel connection between the FC layer and RC frame as reported by Altin et al. (2010). However, for practical strengthening purpose, it is complicated to insert the mesh reinforcement into the RC frame. Therefore, in this study, a new idea has been conceived to secure a connection of the RC frame to wire mesh. The main intension was to make a good attachment of wire mesh to the RC frame, so that wire mesh can actively participate in load transferring. To execute that steel plate and bolt connection has been considered for this study as shown in Fig. 3(c)-(d). The spacing of the bolts has been kept smaller near the RC beam-column joint considering the commencement of separation at that region which might occur without any connection. 12 bolts (8mm in diameter), as shown in Fig. 3(b), have been used along with steel plate with mixed spacing, 100 and 200mm between bolts.

In ferrocement strengthening, wire mesh should also be connected to masonry panel in order to hold it during construction as well as to avoid delamination under lateral loading. Alcocer and Flores (2001) investigated the quantity of optimum connection for ferrocement strengthening of confined masonry and recommended about nine connectors per square meter that have been adopted in this study.

3.2 Test specimen details

Two half-scaled masonry infilled RC frames have been constructed and infill masonry has been strengthened with ferrocement. The overall geometry of the RC frame is shown in Fig. 3(a). The details of both specimens are shown in Table 2. The construction procedure of specimens is as follows: First, the RC frame has been constructed and then masonry panel has been built inside the frame, with solid bricks of 210x100x60 mm, in running bond manner. After seven days of masonry construction, 10mm thick mortar has been mounted on both faces of the masonry wall. This is followed by the attachment of square wire mesh to the RC frame and masonry wall. The wire mesh has been connected to the surrounding RC frame with bolts (inserted into the pre-installed thread) and steel plate as shown in Fig. 3(d). In addition, the wire mesh has been connected with masonry infill by 32mm long nails to hold the wire mesh in place during the application of second layer mortar. The nails have been placed in drilled holes with glue at a horizontal and vertical center to center distance of 250mm and 500mm, respectively. After seven days, the second layer of mortar, having 15mm thickness, has been applied on

the wire mesh. Therefore, FC mortar thickness is about 25mm on each surface of infill masonry.

3.3 Material properties

The material tests of concrete, reinforcing steel have been conducted for each specimen as per Japanese standard (2010). The wire mesh has been tested as per ACI 549R (1997). The masonry compressive strength has been tested according to ASTM (2011). The mechanical properties of concrete, reinforcing steel, masonry, mortar, and wire mesh are shown in Table 3.

Table 2: Details of test specimen

Specimen	RC column (mm x mm)	Wire mesh		
		Diameter, φ (mm)	Spacing, s (mm)	Mesh reinforcement, ρ_{wm} (%)
IM-FC-1	200x200	0.9	5.45	0.16
IM-FC-2		1.6	4.75	0.56

Table 3: Material Properties (all values are in MPa)

Specimen	Concrete compressive strength, f_c'	Reinforcement yield strength, f_y	Masonry		Ferrocement	
			Compressive strength, f_{mas}	Mortar strength, $f_{mor,j}$	Mortar strength, $f_{mor,FC}$	Wire mesh ultimate strength, $f_{u,wm}$
IM-FC-1	24	350	27	37	26	378
IM-FC-2	26		29	35	29	318

3.4 Test setup and instrumentation

Several strain gauges were attached to the long and tie reinforcement of RC column to measure the strain during loading. The locations of the strain gauges are shown in Fig. 4(a). The lateral story deformation of the RC frame is measured by the LVDTs attached to the center of the top beam as shown in Fig. 4(b). Four LVDTs were attached on the top beam (front and back sides) which facilitate in measuring the average story deformation. The story deformation is used to calculate story drift which refers to the ratio of average story deformation to the height of the column. Both specimens have been subjected to cyclic lateral loading and 200kN constant vertical loads on each column to simulate the actual loading on the column in buildings. The schematic diagram of the loading system is shown in Fig. 5, where two pantographs were used to avoid any out-of-plane movement of the frame during loading. The cyclic lateral loading program consisted of two cycles for each lateral drift of 0.05, 0.1, 0.2, 0.4, 0.6, 0.8, 1.0, 1.5, and 2.0%.

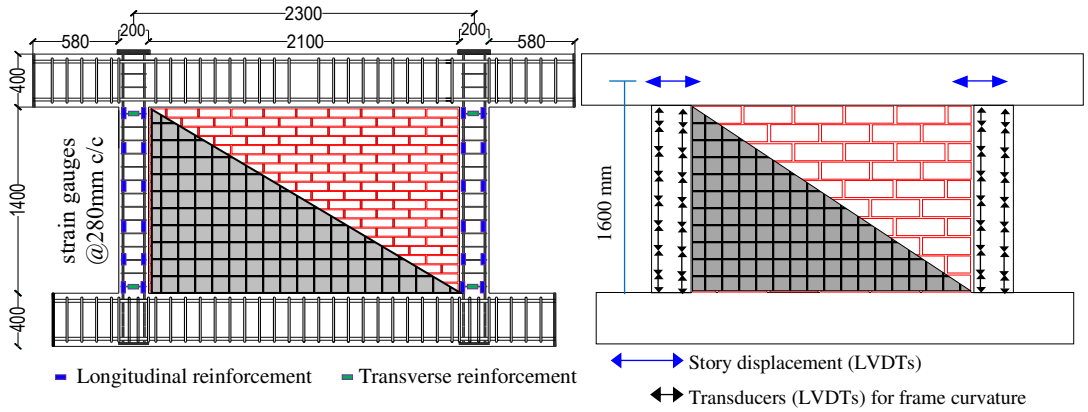

Fig. 4 Location of (a) strain gauges and (b) transducers on columns

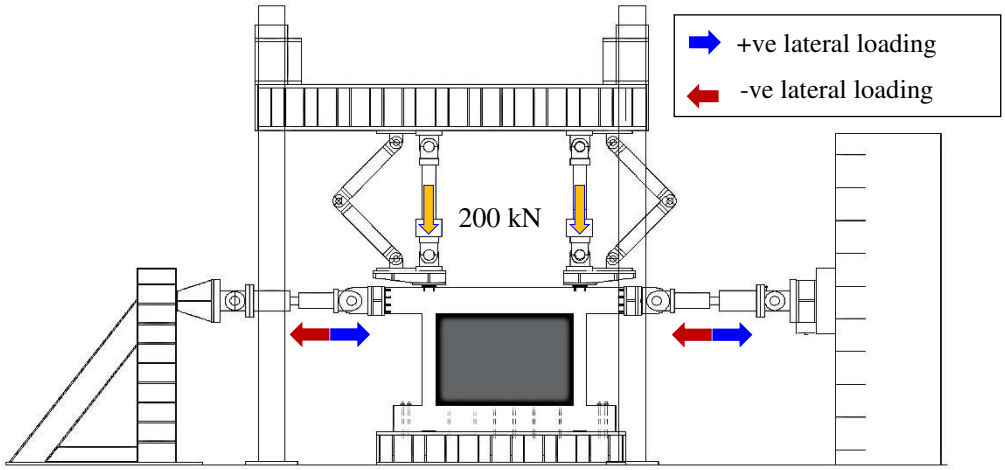

Fig. 5 Test specimen loading system

4 Experimental results

4.1 Crack propagation and damages

Specimen IM-FC-1

At the drift level of 0.05%, cracking was initiated by hairline flexural cracks at the bottom of the tension column and FC strengthened masonry wall. In between 0.1% - 0.2% story drift, the flexural cracks opened more and longitudinal reinforcement yielded at the bottom of the tensile column. The yielding of longitudinal reinforcement was confirmed by the strain obtained from the strain gauges attached to the long reinforcements. The number of flexural cracks on the tension column increased up to the story drift level of 0.4%. At 0.4% story drift, an inclined crack as shown in Fig. 6(a), parallel to compression diagonal, appeared on the FC strengthened infill near the top of the compression column. At around 0.6% drift, wire meshes started to be ruptured in the inclined crack. At this stage, a shear crack also formed at the top of the tension column following sliding at the joint of the strengthened wall and top beam. At 0.8% story drift, all the wire meshes in the inclined cracks were ruptured and the continuous sliding at the top construction joint was clearly observed. Following this more shear cracks were formed at the top of the tension column as shown in Fig. 6(b). At about 1.5% story drift, punching shear failure

of the tension column occurred where column longitudinal reinforcement at the top bent which is followed by full spalling of cover concrete. Loading has been stopped at the 1st cycle of negative 2% lateral drift, where the bottom reinforcement of the compression column buckled which is followed by cover concrete spalling. The final damage state under lateral cyclic loading is shown in Fig. 6(c) and Fig. 7.

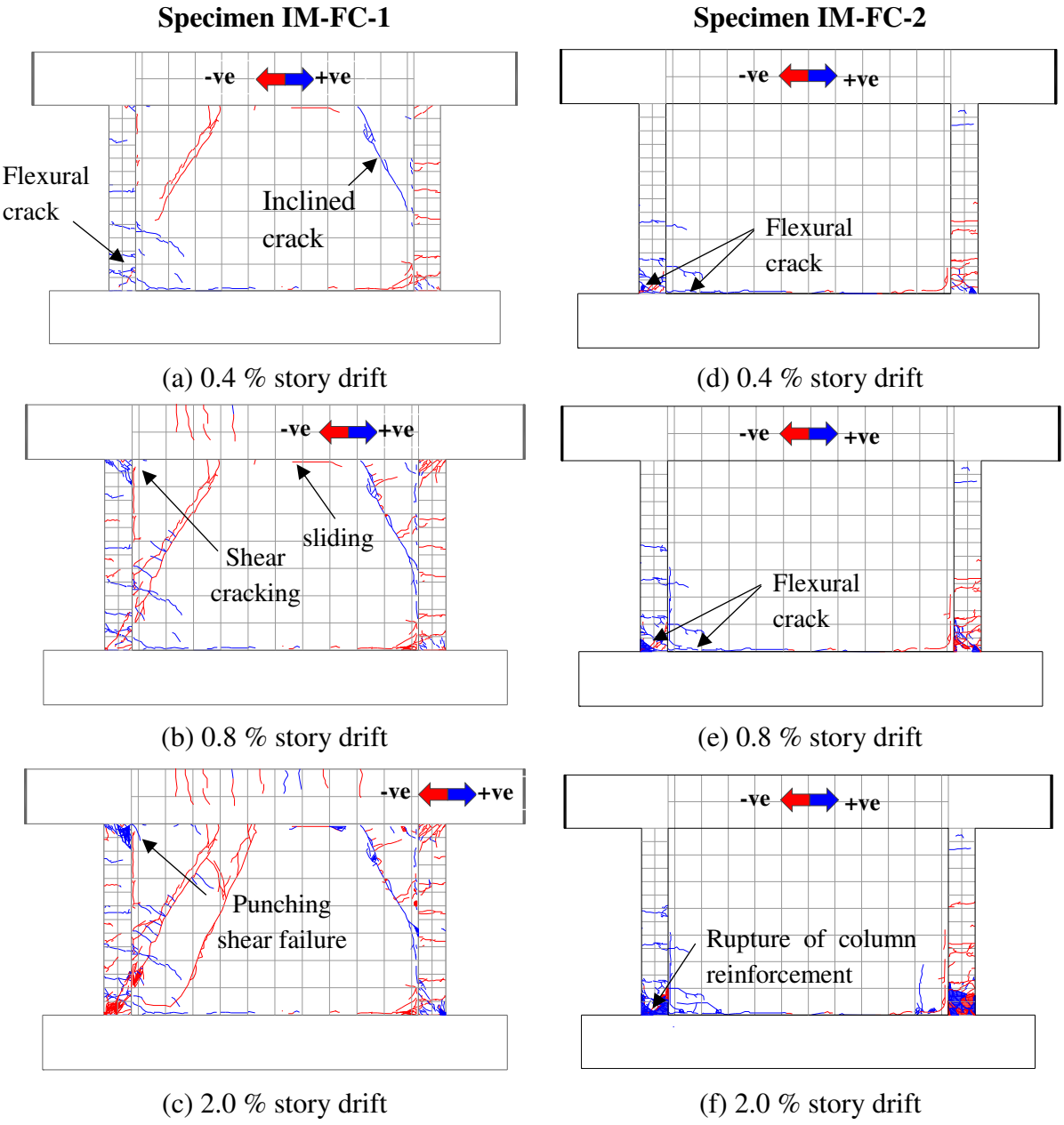

Fig. 6 Crack propagation of specimens (IM-FC-1 and IM-FC-2)

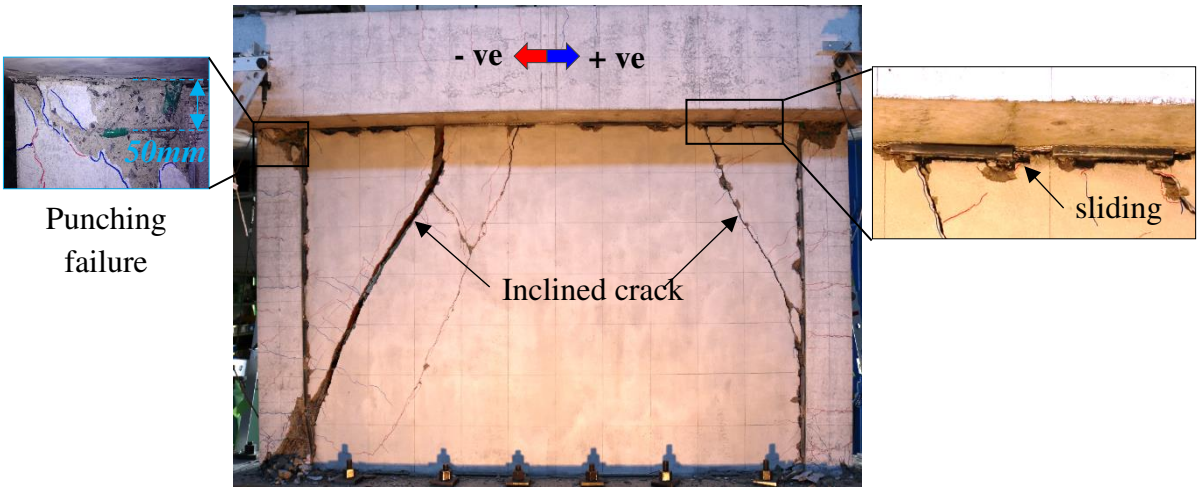

Fig. 7 Final damage state of specimen IM-FC-1

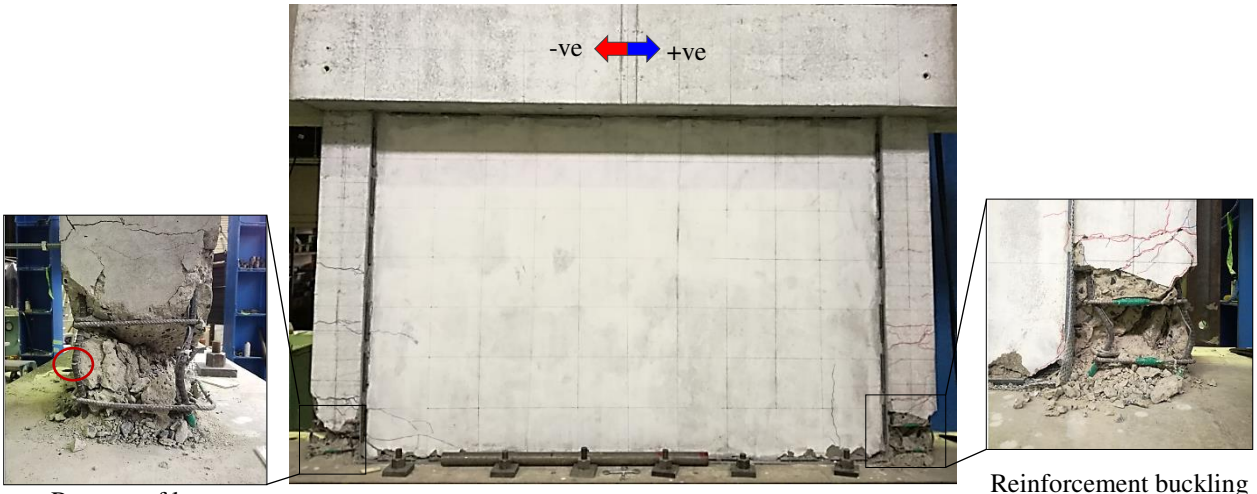

Fig. 8 Final damage state of specimen IM-FC-2

Specimen IM-FC-2

At 0.05% lateral drift, flexural cracking initiated at the bottom of the tension column. The longitudinal reinforcements at the bottom of tension column experienced yielding at 0.1% story drift and confirmed by the strain obtained from the strain gauges attached. At 0.1~ 0.2% story drift, new flexural crack at the joint of wall and stub beam has also been observed. After that, the tension crack width at the bottom of the column gradually increased up to 3mm. At 0.4 ~ 0.8% story drift levels, as shown in Fig. 6(d)-(e), new flexural cracks appeared on the tension column up to the bottom third on the column height and the damages concentrated at the bottom of the compression RC column. At about 1% story drift, the core concrete of the compression column started to be crushed. Wire meshes at the bottom of the wall, which have been connected directly to the beam through steel plate and bolt, started to be ruptured at about 1.5% story drift. Loading has been finished at the 1st cycle of negative 2% lateral drift, where three out of four main reinforcements of the tension column ruptured. The final crack pattern under

lateral cyclic loading is shown in Fig. 6(f) and Fig. 8. It is to be noted that no other crack, except at the bottom horizontal crack, was observed on the FC strengthened masonry infill. In addition, there was no crack at the top construction joint.

4.2 Response under cyclic lateral load

Specimen IM-FC-1

The hysteresis loops of IM-FC-1 is shown in Fig. 9(a). The response was essentially linear up to the formation of the first crack on the tension column at 0.05% story drift. After cracking, the hysteresis loops began to wide, specifically after 0.4% story drift when an inclined crack appeared on the ferrocement laminated masonry. The peak resistances were +538kN and -530kN at the story drift of +0.39% and -0.38, respectively. After peak resistance, the stiffness of the hysteresis loop gradually increases with load enhancement, exhibiting a "pinching" in the hysteresis curve. This could be attributed to the sliding at the top joint as discussed before. At around 0.6% drift, a sudden drop in lateral resistance occurred following the sliding at the top construction joint. As the sliding continues, the residual resistance of the specimen became almost constant which is marked by the horizontal post-peak branch of the envelope curve as shown in Fig. 9(a). The story drift capacities at residual strength are 0.55 and 0.56 in positive and negative loading directions, respectively. The residual capacity is considered at the 80% of peak resistance on the post-peak branch.

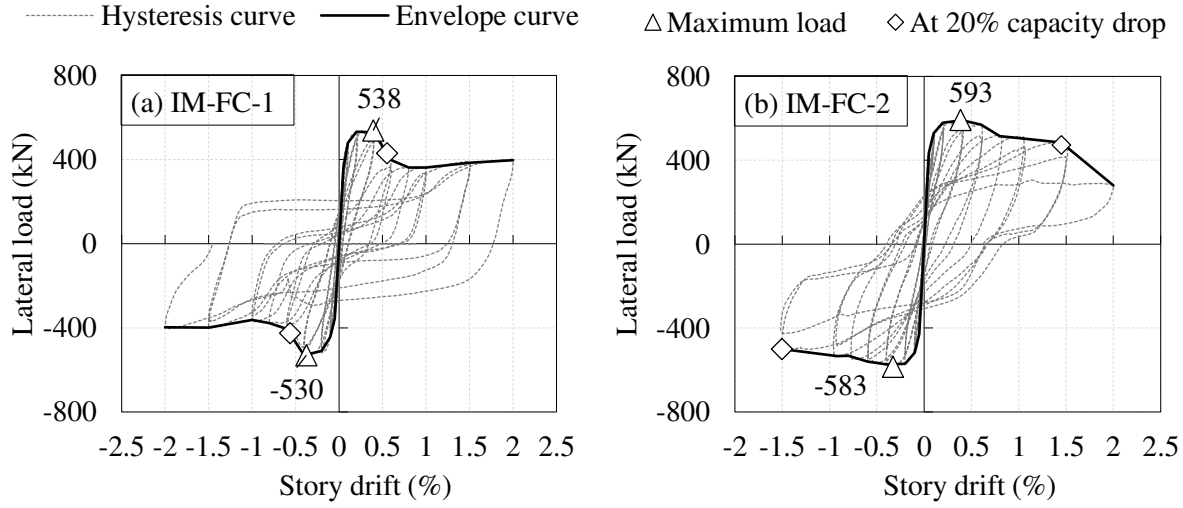

Major incidents (IM-FC-1)

0.1~0.2%: *main bars in tension columns yielded*
0.4%: *peak load resistance and inclined crack on wall*
0.6%: *shear crack at tension column's top and sliding started at top of wall*
1.5%: p*unching shear failure at tension column top*

Major incidents (IM-FC-2)

0.1%: *main bars in tension columns yielded*
0.4%: p*eak load resistance*
1.5%: *wire mesh at bottom of tension side ruptured and compression column bottom concrete crushed*
2%: *three out of four main reinforcements of tension column ruptured*

Fig. 9 Lateral load-story drift relationship of specimen IM-FC-1 and IM-FC-2

Specimen IM-FC-2

The hysteresis loops of IM-FC-2 is presented in Fig. 9(b). The behaviour was essentially elastic until the formation of the initial crack on the tension column at 0.05% story drift. After cracking, the relatively stiffer hysteresis loops continued until the specimen IM-FC-2 reached to the peak resistance of +593kN and -583kN at the story drift of +0.38% and -0.33, respectively. The stiffness upon increasing lateral displacement gradually decreases and forming a fatter hysteresis loop indicating absorption of a large amount of hysteretic energy. The lateral resistance also gradually decreased by reflexing the damage concentration at the bottom of both RC columns. The story drift capacities at residual strength capacity are 1.45 and 1.5 in positive and negative loading directions, respectively.

4.3 Recognition of failure mechanism

The failure mechanism i.e. load transfer mechanism at peak resistance is necessary to be identified for lateral strength evaluation that is to be discussed in the next section. The aforementioned crack propagation and hysteresis behaviour, indicate that specimen IM-FC-1 undergone both flexural and shear damages whereas IM-FC-2 mostly undergone through flexural behaviour throughout the courses of lateral story drift. However, the following analysis were conducted to recognize the load transfer mechanism at the peak resistance.

Shear and flexural component of story deformation

The flexural and shear components of total lateral deformation were measured to confirm the failure modes of the specimens. The flexural component (Δ_{flex}) of lateral story deformation was measured using the LVDTs attached over the height of RC columns as shown in Fig. 4(b). At a certain lateral story deformation, the flexural story deformation can be calculated as per Eq. (1) which is theoretically area under the rotation diagram. The rotation at each section (LVDTs were attached) was calculated using Eq. (2) where vertical displacements of tension ($\delta_{TC,i}$) and compression ($\delta_{CC,i}$) columns were measured by taking the average displacement of pair of LVDTs attached on each section column. In Eq. (2), L indicates the center to center column distance. The shear component (Δ_{shear}) of lateral story deformation was measured using Eq. (3) assuming lateral story displacement is the summation of the flexural and shear displacement. The average story deformation (Δ_{story}) was measured using the transducers attached to the top beam as discussed in the last section.

$$\text{Flexural deformation, } \Delta_{flex} = \int \theta \, dh \tag{1}$$

$$\text{Rotation at } i^{\text{th}} \text{ –section, } \theta_i = \frac{\delta_{TC,i} - \delta_{CC,i}}{L} \tag{2}$$

$$\text{Shear component of lateral story deformation, } \Delta_{sh} = \Delta_{story} - \Delta_{flex} \tag{3}$$

The obtained flexural and shear deformation in relation to the story drifts are shown in Fig. 10(a)-(b). In specimen IM-FC-1, the flexural contribution is relatively more at lower story drifts as shown in Fig. 10(a). At higher story drifts, the tension column experienced punching shear failure following sliding at the top joint which led to an increase in shear deformation. Another strengthened RC frame, namely IM-FC-2, experienced flexure domination throughout the course of the lateral drift as shown in Fig.10(b). In other words, IM-FC-1 behaved as a flexural wall at the drift lower than 0.4% and then failed in punching shear of the tension column, however the specimen IM-FC-2 behaved like a flexural wall for all story drifts.

Rotation at the top of tension column

In specimen IM-FC-1, at higher story drift level the tension column was failed in punching shear where the long reinforcement bent at the level of tie reinforcement as shown in the close view of Fig. 7. Therefore, the rotation of four column sections, where LVDTs were attached, on the upper half of the tension column are investigated as shown in Fig. 11(a). It is obvious that until 0.2% story drift there was almost no rotation at the column sections on the upper half of the tension column. Then, rotation at the top column section, at level 1380mm from the base, increased gradually leading to the reinforcement bent i.e. punching shear failure at around 1.5% story drift. In specimen IM-FC-2, there was no visible sliding at the top construction joint, as discussed earlier, therefore no trace of punching shear failure i.e. long reinforcement bent was found. However, the rotation at the aforementioned four column sections on the upper half of the tension column is investigated as shown in Fig. 11(b) to confirm the fact. It is obvious that there was almost no rotation at the top column section at level 1380mm from the base, hence no punching shear damage of the tension column.

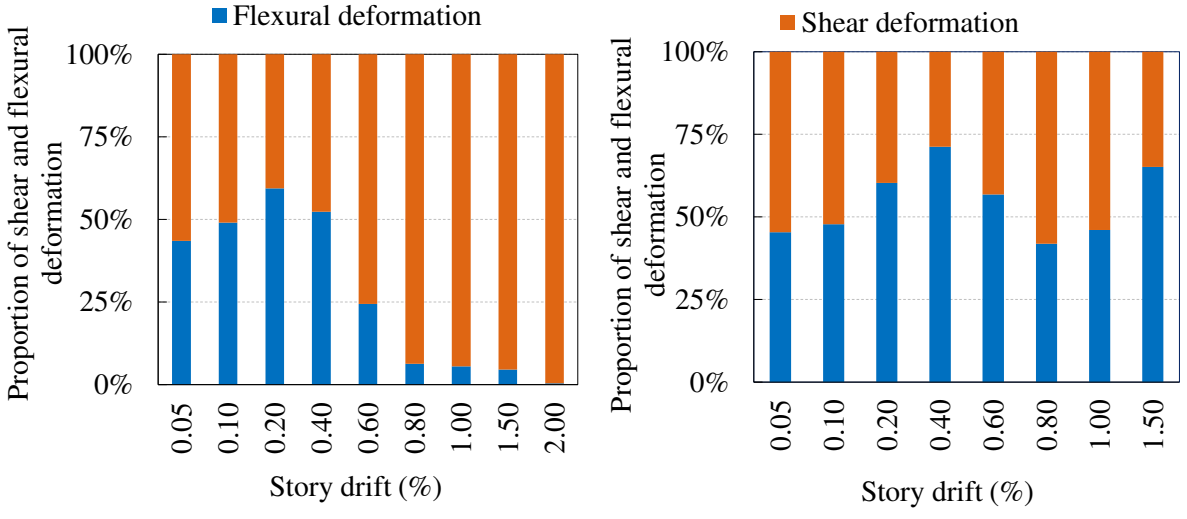

(a) Specimen IM-FC-1 (b) Specimen IM-FC-2

Fig. 10 Flexural and shear components of story deformation of specimen IM-FC-1 and IM-FC-2

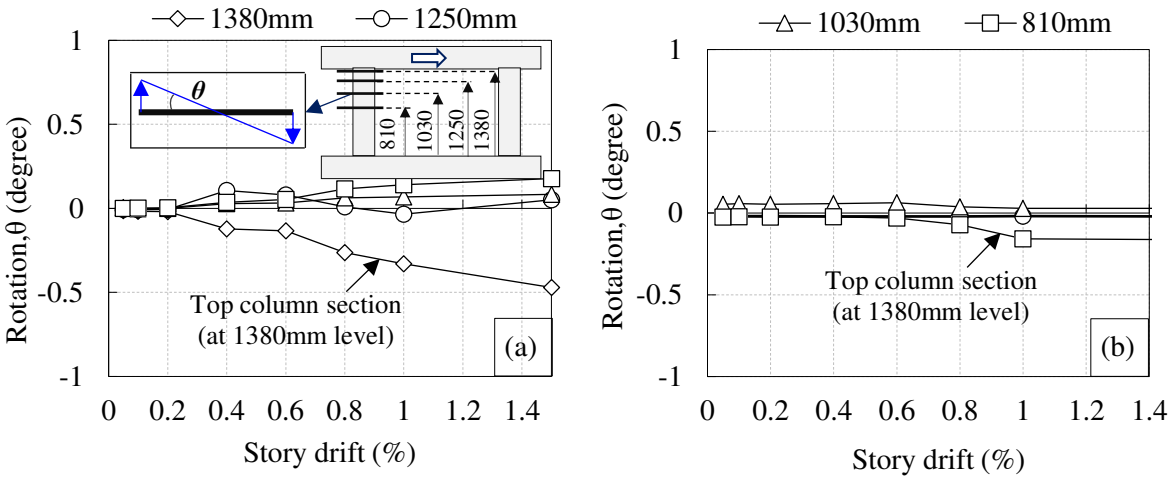

Fig. 11 Rotation of tension column at several sections of specimen IM-FC-1 and IM-FC-2

From the above two analyses, it is clear that the specimen IM-FC-1 started to rock at lower story drifts levels, until 0.4% story drift, like a structural wall with boundary columns. At higher story drifts, the rocking behavior was ceased due to the sliding at the top construction joint which ultimately leads to punching shear failure of the tension column. Therefore, the load transfer mechanism is idealized as an overall flexural failure at peak resistance. On the other hand, specimen IM-FC-2 started to rock from the beginning and continued rocking behavior until failed with rupture of long reinforcement of the tension column. Therefore, the failure is idealized as fully developed overall flexural failure.

5 Lateral strength evaluation

5.1 Recognized major failure mechanisms

As discussed earlier, the failure mechanism of the infilled RC frame depends on relative stiffness as well as the strength of infill material compared to the surrounding RC frame. When relatively weak masonry infill is strengthened with ferrocement, failure initiates on the infill panel by diagonal compression crushing (Kaya et al. 2018 and Demirel et al. 2015) or diagonal cracking and/or sliding (Seki et al. 2018, Altin et al. 2010, Zarnic and Tomazevic 1985) as recognized from past experimental studies. However, when strong masonry is strengthened with ferrocement, the RC frame could be the weakest part and consequently can fail by overall flexural or column punching leaving the infill panel undamaged as observed in the current experimental program. In addition, two other specimens from author's other publications, namely AR (Alwashali et al. 2020) and IM-FC (Zahura et al. 2020), are utilized herein in the lateral strength evaluation and ductility sections. Both specimens (AR and IM-FC) were failed by column punching and joint sliding.

Based on the current experimental observation and previous studies four distinct major failure mechanisms, as shown in Fig. 12, are recognized.

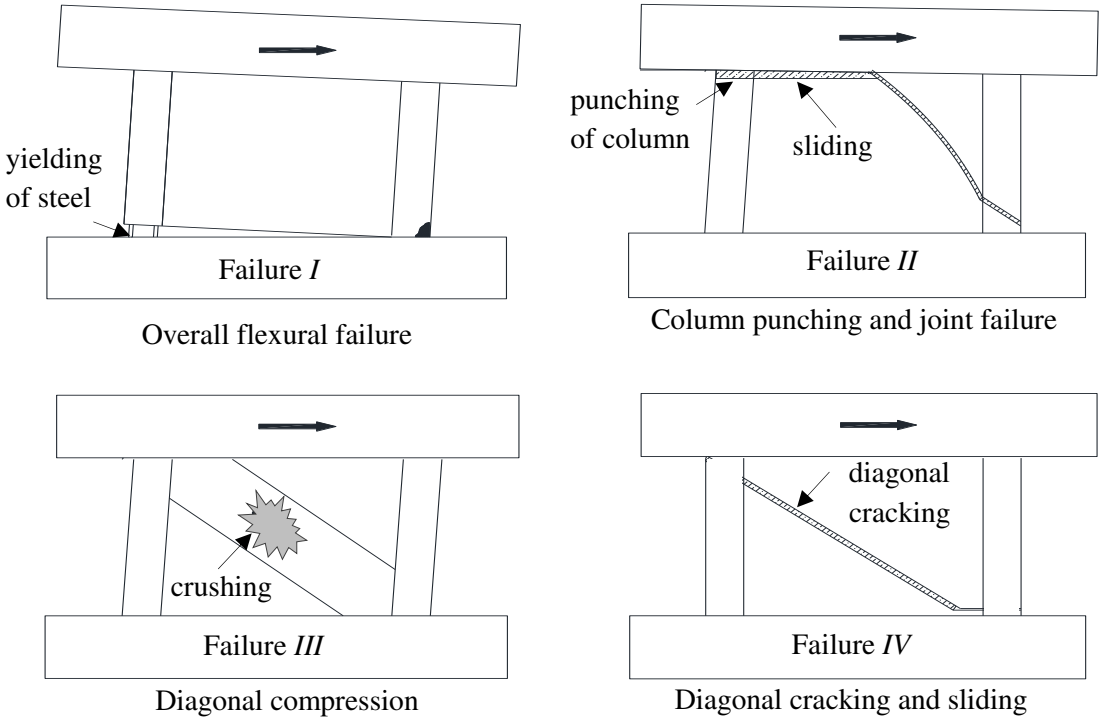

Fig. 12 Major failure mechanisms of FC strengthened masonry infilled RC frame

5.2 Lateral strength evaluation of each failure mechanism

Overall flexural (Failure I)

Overall flexural failure is likely to occur when the infill panel (masonry and FC layer) is very strong and stiff. This phenomenon can be attributed to the fact that when the infill panel is very strong and stiff, it cannot deform in a shear mode therefore the structural system undergoes a rocking mode like a rigid body. This rocking behavior generates tensile yielding of the tension column longitudinal reinforcements followed by failure due to rupture of longitudinal reinforcement of the tension column (left side close view in Fig. 13), and concrete crushing at the bottom of the compression column (right side close view in Fig. 13).

The idealized load transfer mechanism by overall flexural yielding is shown in Fig. 13. The lateral capacity at flexural yielding of RC frame (Q_I) is computed from flexural theory, using Eq. (4) and Eq. (5). It is to be noted that the contribution of mesh reinforcement is not considered in ultimate moment calculation (Eq. (5)) because all mesh reinforcements were not connected through the steel plate and bolt with stub/foundation beam. In addition, if dowel bars are used, it might not contribute like shear wall reinforcement because of the discontinuity of those bars (i.e. not having enough development length to sustain stretching/yielding). Therefore, the lateral capacity of the cantilever wall is thought to be provided by the only RC frame.

$$Q_1 = {}^{M_u}/_{h_o} \tag{4}$$

$$M_u = a_t f_y l_c + 0.5 N l_c \tag{5}$$

where, M_u = ultimate moment capacity of RC frame; h_o = clear height of column; a_t = cross sectional area of column longitudinal reinforcements; f_y= yield strength of column longitudinal reinforcement; l_c = c/c distance of boundary columns, and N = axial load on RC columns (=2N').

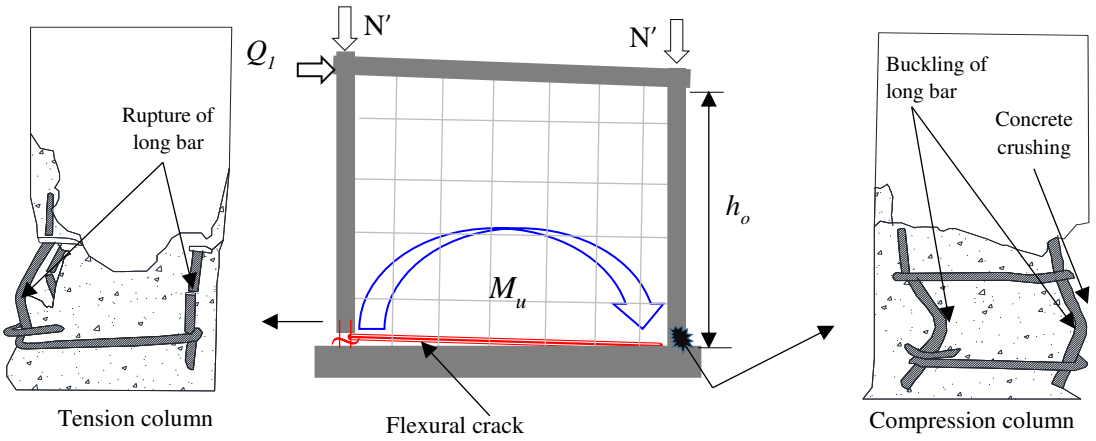

Fig. 13 Load transfer mechanism of overall flexural failure (Failure I)

<u>Column punching and joint sliding</u> (Failure II)

Column punching-joint sliding failure is also likely to occur when the infill panel (masonry and FC layer) is very strong and stiff compared to the RC frame. However, in this case, failure triggering incident is sliding at the top construction joint. Sliding occurs at the top construction joint, then the tension column might fail in shear. The shear failure of the column is concentrated within a very short distance from the bottom face of the top beam. For example, shear failure of tension column concentrated with 50mm from the top beam face in the case of specimen IM-FC-1 as shown in the close view of Fig. 14. The idealized load transfer mechanism of FC strengthened masonry infilled RC frame at top construction joint failure and column punching is shown in Fig. 14, which occurred in the current experimental program specimen IM-FC-1 at higher story drifts and specimen AR (Alwashali et al. 2020) and IM-FC (Zahura et al. 2020). The total shear capacity (Q_2) can be evaluated by Eq. (6).

$$Q_2 = {}_{ps}Q_c + {}_{js}Q_w + {}_{f}Q_c \tag{6}$$

where, ${}_{ps}Q_c$ = punching shear resistance of tension column; ${}_{js}Q_w$ = shear resistance at top construction joint, and ${}_{f}Q_c$= flexural shear resistance of compression column.

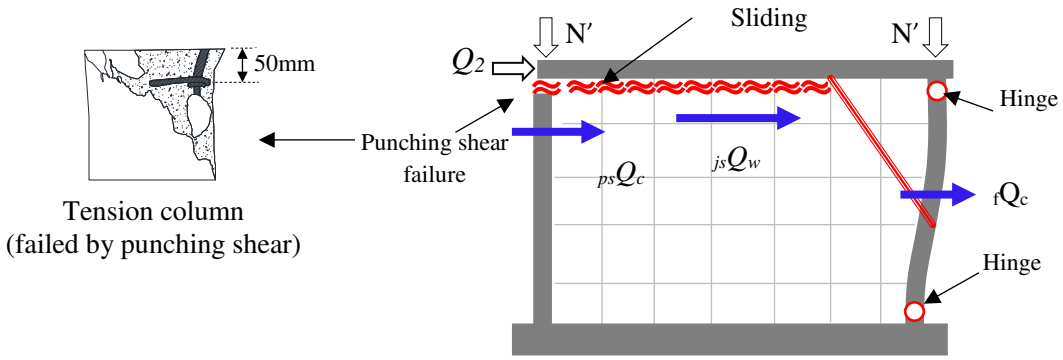

Fig. 14 Idealized load transfer mechanism of column punching and joint failure (Failure II)

Generally, punching shear failure occurs at the top end of the tension column, as explained prior in Fig. 14, within a very short distance from the face of the top beam. Therefore, this type of shear failure is known as an extremely short column (JBDPA 2001) where the shear span ratio is less than unity. Since the shear span ratio is very low, hence the shear failure is considered alike to slippage (Yamamoto 1990) where shear resistance comes more likely from shear friction rather than shear reinforcement. The punching shear capacity ($_{ps}Q_c$) of the column is determined based on the procedure suggested by JBDPA (2001). In JBDPA (2001), punching shear capacity is evaluated by Eq. (7). In evaluation, the basic shear strength (τ_o) is computed, using Eq. (8) – Eq. (10), based on shear friction (Yamamoto 1990) i.e. taking into account the influence of long reinforcement and axial stress level on the shear plane. However, to include the influence of shear span ratio (a/d), an influence factor (k_{min}) has also been considered in Eq. (7), as suggested by Yamamoto 1990 as per Eq. (11). The shear span ratio (a/d) is considered equal to 1/3 for all the specimens as suggested by JBDPA (2001) standard for this kind of punching shear failure. Lateral capacity of the compression column ($_fQ_c$) can be computed as per JBDPA (2001) using Eq. (12).

$$_{ps}Q_c = k_{min}\tau_o bd \tag{7}$$

$$\tau_o = 0.98 + 0.1f_c + 0.85\sigma \quad \text{in case } 0 \le \sigma \le 0.33f_c - 2.75 \tag{8}$$

$$= 0.22f_c + 0.49\sigma \quad \text{in case } 0.33f_c - 2.75 \le \sigma \le 0.66f_c$$

$$= 0.66f_c \quad \text{in case } 0.66f_c \le \sigma$$

$$\sigma = \rho_g f_y + \sigma_0 \tag{9}$$

$$\sigma_0 = \frac{N'}{bd} \tag{10}$$

$$k_{min} = \frac{0.34}{0.52 + {}^{a}/_{d}} \tag{11}$$

$$_fQ_c = \frac{2M_c}{h_o} \tag{12}$$

where, where, K_{min} =influence factor considering shear span ratio; τ_o = basic shear strength of column; b and d = width and depth of column; a = shear span = $d/3$; ρ_g = longitudinal reinforcement ratio of column, f_c = concrete compression strength, f_y = yield strength of longitudinal reinforcement, N'= axial load on each column; M_c = moment capacity of RC column; h_o = clear height of column.

The source of joint shear capacity ($_{js}Q_w$) could be the masonry joint mortar, mortar of the FC layer, and embedded wire meshes in the FC layer. From the lateral behavior of specimen IM-FC-1, it is clear that initially shear strength is greater than flexural capacity (i.e. shear failure after flexural yielding) and the lateral resistance degraded 25% after occurring slippage at the top construction joint. This indicates that initially, the bond between FC laminated masonry and soffit was working. Then, after slippage, wire meshes were working as a dowel to provide residual capacity. Therefore, at the initial stage, before any slippage at the interface of infill top and soffit, shear capacity can be considered as shear strength (cohesion) of mortar at the interface. In initial bond capacity, wire mesh might have a contribution in addition to mortar cohesion however, as a conservative approach wire mesh contribution is ignored. After the occurrence of slippage wire mesh will be subjected to shearing force hence can be considered as the source of residual shear capacity at the interface. The joint shear capacity can be evaluated from Eq. (13).

$$_{js}Q_w = \tau_{mas} l_w t_{mas} + \tau_{mor,FC} l_w n_s t_{FC} \tag{13}$$

where, $_{js}Q_w$ = shear capacity at joint; τ_{mas}, $\tau_{mor,FC}$ = shear strength (cohesion) of mortar in masonry joint and ferrocement; l_w = length of infill; t_{mas} , t_{FC} = thickness of masonry wall and FC layer; and n_s = number of FC surface. It is to be noted that cohesion capacity of mortar, for both masonry and FC layer, has been considered as $0.17\sqrt{f_{mor}}$ (where f_{mor} =compressive strength of mortar), which has been recommended by Naaman (2000), and Mander and Nair (1994) as shear strength of FC.

<u>Diagonal compression</u> (Failure III)

In diagonal compression failure, the infilled part (masonry and FC layer) is considered to behave similarly to a diagonal strut, as shown in Fig. 15, that would fail by compression crushing. In addition, flexural hinges would form at the top and bottom ends of RC columns. The lateral strength (Q_3) can be evaluated by using Eq. (14).

$$Q_3 = 2\ {}_fQ_c + \left(0.5 f_{m,90} W_s t_{mas} + 0.5 f_{mor,FC} W_s n_s t_{FC}\right) Cos\theta \tag{14}$$

where, $_fQ_c$= flexural shear resistance of RC column; $f_{m,90}$ = expected prism compressive strength of masonry in horizontal direction (= 0.5 x masonry prism compressive strength, f_m (ASCE/SEI 41-06 2007); $f_{mor,FC}$ = FC mortar compressive strength; W_s = strut width of FC laminated masonry; t_{mas}, t_{FC} = thickness of masonry and FC mortar layer; n_s = number of surface retrofitted with FC, and θ = inclination of loaded diagonal with horizontal.

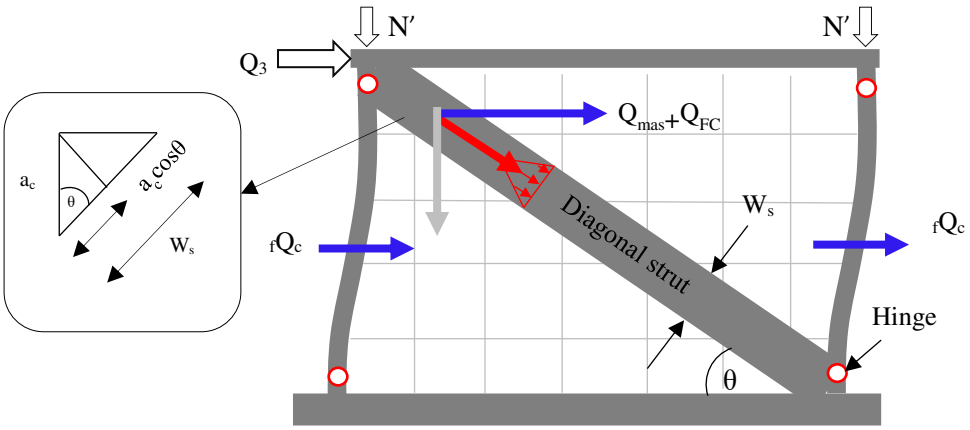

* Q_{mas} + Q_{FC} = sum of horizontal components of masonry and FC mortar contribution

Fig. 15 Idealized load transfer mechanism of diagonal compression failure (Failure III)

In Eq. (13), the flexural capacity of the RC column ($_fQ_c$) can be evaluated using Eq. (12). Other parameters in Eq. (14), except diagonal strut width (W_s), are mostly related to masonry and FC materials and geometry. The strut width (W_s) depends on the relative rigidity of infill material in comparison to the surrounding RC column (Smith 1966). The diagonal strut (W_s) width is considered in terms of contact length (a_c) between the RC column and infill panel as per Eq. (15) in reference to Fig. 15.

$$W_s = 2a_c cos\theta \tag{15}$$

where, W_s = strut width; a_c = contact length between RC column and infill panel; and θ = inclination of loaded diagonal with horizontal. The contact length is calculated by considering that the RC column is resting on an infill panel, as shown in Fig.16(a), similar to a beam on an elastic foundation (Hetenyi 1946). Therefore, lateral deflection (y) and curvature (φ) of the RC column can be evaluated considering it is analogous to a beam on an elastic foundation, as shown in Fig. 17(b) and 17(c).

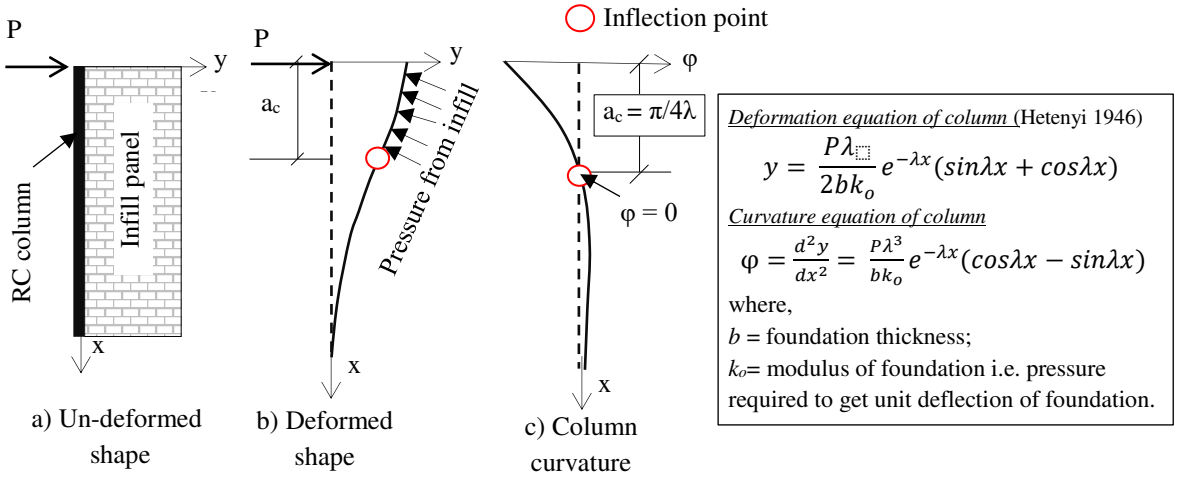

Fig. 16 Surrounding RC column (a) un-deformed shape, (b) deformed shape and (c) curvature distribution

Relative rigidity (λ) of infill panel with respect to RC column is defined as Eq. (16).

$$\lambda = \sqrt[4]{\frac{(E_{mas}t_{mas}+E_{FC}n_s t_{FC})\cos^2\theta}{4E_C I_c d_m}} \tag{16}$$

where, λ = relative rigidity factor for FC strengthened masonry, θ = inclination of loaded diagonal with horizontal; E_c, E_{mas}, E_{FC} = Young's modulus of concrete, masonry, FC mortar; t_{mas}, t_{FC} = thickness of masonry, FC mortar layer; n_s = number of surface retrofitted with FC; I_c = moment of inertia of RC column; and d_m = diagonal length of infill panel.

It is evident from the column deflection shape, as shown in Fig. 16(b), that the lower portion of the RC column exhibits flexure deflection whereas the deflection mode of the upper part is changed from a flexural shape due to the presence of infill masonry, which actually causes the separation between masonry and RC frame. Based on the deflection shape, it is considered that the infill panel of the upper part of the inflection point is attached with RC frame effectively and considered as the contact length (a_c) of diagonal strut. The height of inflection point i.e. contact length (a_c) is evaluated from the condition of zero curvature at the inflection point, as shown in Fig. 16(c), using Eq. (17).

$$a_c = \frac{\pi}{4\lambda} \tag{17}$$

<u>Diagonal cracking and sliding</u> (Failure IV)

In case of diagonal cracking and sliding failure, at lower story drifts level, a diagonal tensile crack appeared on FC strengthened infill panel, as shown in Fig. 17(a). However, at post-peak stage the strengthened masonry can have a sliding behavior as shown in Fig. 17(b). Therefore, this failure mechanism is defining as diagonal cracking and sliding failure.

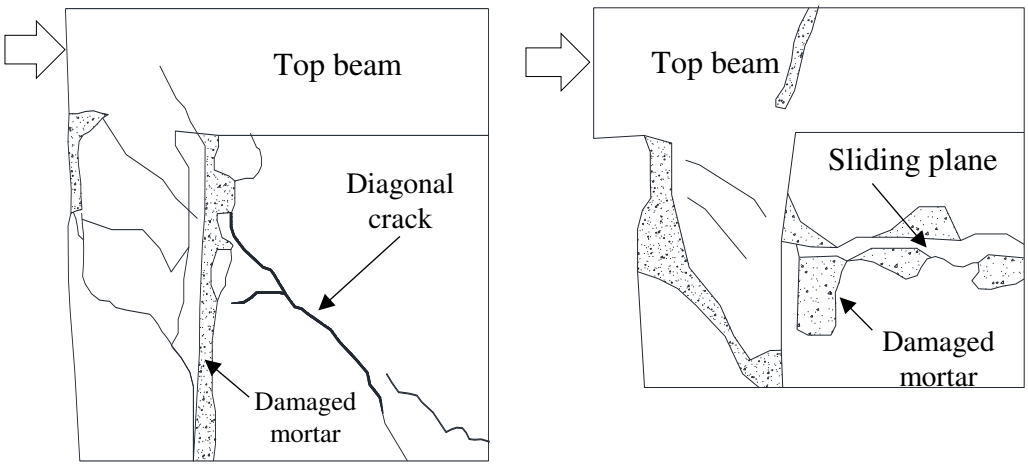

(a) Diagonal cracking at peak resistance

(b) Sliding at post peak stage

Fig. 17 Damage (a) at peak resistance (back view) and (b) at post peak stage (front view) of specimen S5-FMFC (Seki et al. 2018)

Since peak resistance occurs at the diagonal cracking stage, therefore the idealization of the load transfer mechanism at the peak is considered as shown in Fig. 18. The FC strengthened masonry cracked on the loaded diagonal direction whereas the frame behaves like a bare frame. At diagonal cracking, lateral strength can be evaluated, as a summation of the strength of RC columns, masonry, and wire meshes of ferrocement, using by Eq. (18).

$$Q_4 = 2\ {}_fQ_c + f_{mas,cr}A_{mas}sin\theta + \alpha.n_s n_L \frac{A_{wm}}{S_v}.f_y.h_{mas} \tag{18}$$

where, ${}_fQ_c$ = lateral capacity of RC column (can be evaluates from Eq. (11)), where, $f_{mas,cr}$ = cracking strength of infill masonry, A_{mas} = diagonal area of infill masonry (diagonal length x thickness), θ = angle of diagonal with horizontal, A_{wm} = area of wire mesh, S_v = vertical spacing of wire mesh, f_y = yield strength of steel wire mesh, h_{mas} = height of wall, α = empirical reduction factor, n_s = number of FC laminated surfaces, and n_L= number of wire mesh layer in each FC layer.

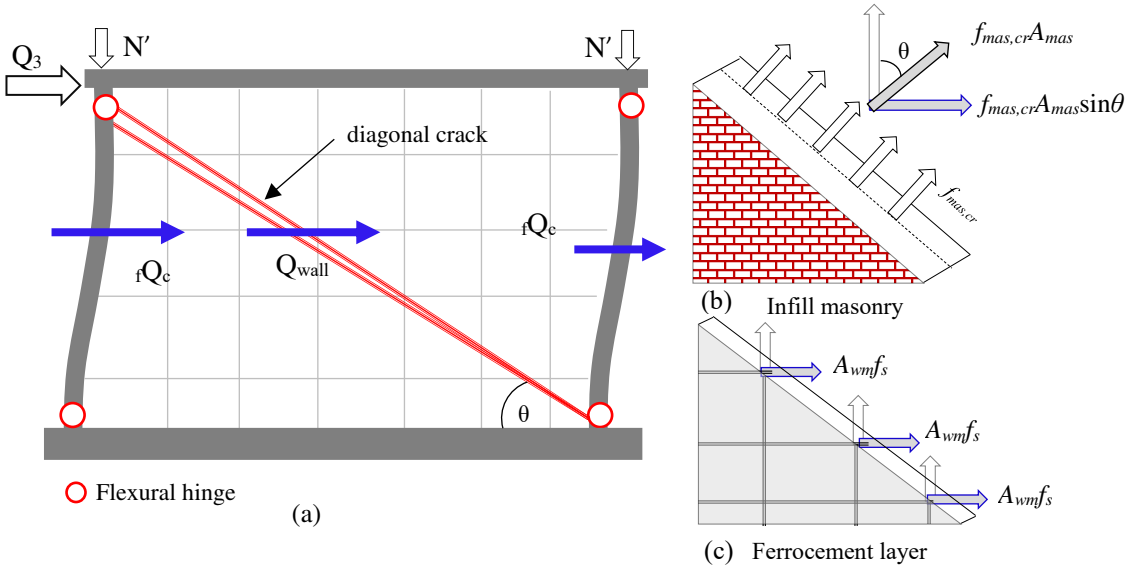

Fig. 18 (a) Idealized load transfer mechanism of diagonal cracking and sliding (Failure IV) (b) cracked infill masonry and (c) cracked ferrocement layer

The contribution of infill masonry due to diagonal cracking has been evaluated by the second term of Eq. (18), in reference to Fig. 18(b). Masonry cracking strength ($f_{mas,cr}$) is considered as 5% of masonry compressive strength (Sen 2020), which has been proposed based on diagonal wallet test results. The contribution of ferrocement has been considered as the shear capacity provided by the horizontal wire meshes as the third term of Eq. (18). The contribution of FC mortar layer in cracking capacity is not considered assuming the fact that the mortar and wire mesh will not work together because FC layer mortar would crack before wire meshes come into tension. Conceptually, the contribution of horizontal wire meshes is assumed like reinforcements in a RC wall. However, Alcocer et al. (2003) found that the strain in reinforcement at the central portion of the reinforced masonry wall is greater compared to the strain near the corner, which implies that all of the horizontal reinforcements of diagonal crack

might not reach to yield condition. Assuming the similar behavior for the ferrocement strengthened masonry, an empirical reduction factor (α) has been imposed in Eq. (18) to accommodate the less effectiveness of mesh reinforcement compared to contribution in the RC shear wall. The less effectiveness might happen due to the less development length provided for reinforcements in masonry. Anderson and Priestley (1992) observed that the strength of shear reinforcement in a reinforced masonry wall is approximately half than that of in RC shear wall. Several building codes e.g. MSJC (2011); CSA-S304.1 (2004) and NZS 4230 (2004) have also taken account less effectiveness of horizontal reinforcement for internally reinforced masonry. The range of the reduction factor varies in between 0.5 ~ 0.8. In this study, the empirical reduction factor (α) has been assumed as 0.7 for ferrocement lamination as suggested in Sen et al. (2020).

5.3 Proposal and validation on lateral strength evaluation

Since, masonry infilled RC frame with ferrocement strengthening can undergo several load transfer mechanisms, as discussed in the earlier section, therefore it is important to recognize the expected load transfer mechanism which likely to occur under lateral loading at seismic events. In general, the expected load transfer mechanism should be the one with the lowest lateral resistance. Therefore, the expected lateral strength (Q_{cal}) will be the minimum of the capacities of all load transfer mechanisms as shown in Eq. (19).

$$Q_{cal} = min\ (Q_1, Q_2, Q_3, and\ Q_4) \tag{19}$$

where, Q_1 = lateral capacity at overall flexural failure; Q_2 = lateral capacity at column punching and joint sliding failure; Q_3 = lateral capacity at diagonal compression failure and Q_4 = lateral capacity at diagonal cracking and sliding failure.

All the calculated lateral capacities and experimental capacities are presented in Table 4. In the case of overall flexural (specimen IM-FC-2), diagonal compression (specimen Sp-5 (Kaya et al. 2018) and SMF (Demirel et al. 2015)), and diagonal cracking-sliding (specimen S5-FMFC (Seki et al. 2018), Sp-4 (Altin et al. 2010), and M3 (Zarnic and Tomazevic 1985)) load transfer mechanism, the minimum calculated capacity can predict the failure mechanism. In case of mixed failure (specimen IM-FC-1) and column punching-top joint sliding failure (specimen AR (Alwashali et al. 2020) and IM-FC (Zahura et al. 2020)) the predicted failure mechanism deviates from the actual failure mechanism. Therefore, it can be concluded that in most cases the proposed evaluation method can predict the failure mechanism.

In addition, the calculated lateral strength (Q_{cal}) and experimental lateral strength (Q_{exp}) for all the investigated specimens are plotted in Fig. 19. In almost all the cases the prediction is on the safe side. The average calculated to experimental capacity ratio (Q_{cal}/ Q_{exp}) is 0.8 with a coefficient of variation 0.2.

Table: 4: Summary of the experimental and calculated lateral strengths

Specimen	Experimental		Calculated capacities				Predicted capacity	
	Observed failure	Q_{exp}	Q_1	Q_2	Q_3	Q_4	Q_{cal}	Q_{cal}/Q_{exp}
		kN	kN	kN	kN	kN	kN	
IM-FC-1	Mixed	538	494	487	612	337	337	0.63
IM-FC-2	Overall flexural	593	494	492	649	502	492	0.83
AR (Alwashali et al. 2020)	Column punching and joint sliding	942	1332	832	1322	557	557	0.59
IM-FC (Zahura et al. 2020)		176	260	178	137	142	137	0.78
Sp-5 (Kaya et al. 2018)	Diagonal compression	155	212	174	110	200	110	0.71
SMF (Demirel et al. 2015)		181	700	280	136	-	136	0.75
S5-FMFC (Seki et al. 2018)	Diagonal cracking and sliding	330	680	334	302	300	300	0.91
Sp-4(Altin et al. 2010)		191	217	136	237	114	114	0.59
M3 (Zarnic and Tomazevic 1985)		333	1300	427	472	375	375	1.12
							Average =	0.77
							Coefficient of variation (CoV) =	0.21

* Mixed failure refers to flexural yielding then column punching and joint sliding

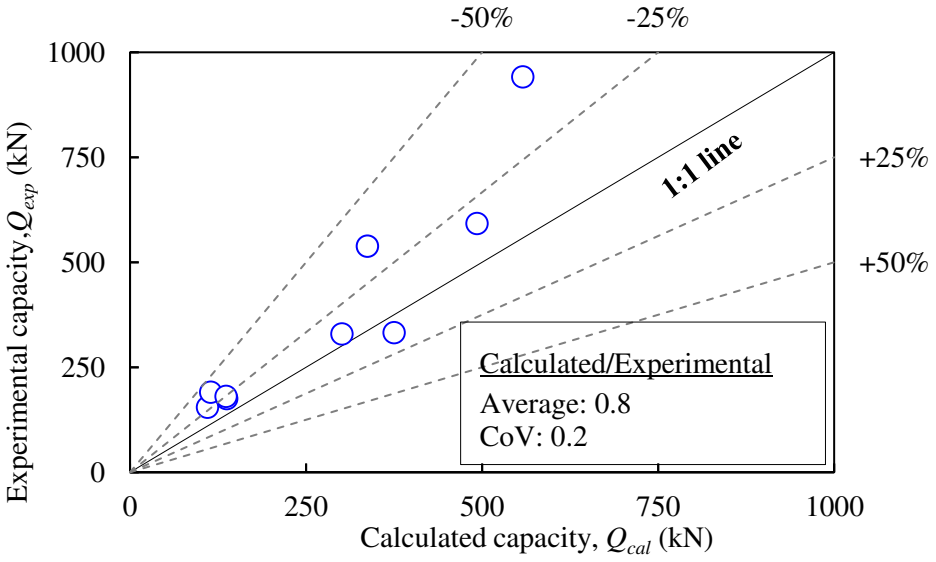

Fig. 19 Calculated and experimental capacities all investigated specimens

6 Comparison of ductility level for all failure mechanisms

Ductility of a structure indicates the capability of that structure to undergo large inelastic deformation without a substantial reduction in lateral strength. There are several parameters, e.g. absorbed energy and lateral displacement, to define ductility. In this study, displacement ductility factor (μ) ductility is considered as the ratio of ultimate and yield lateral story drift as shown in Eq. (20).

$$\mu = \frac{R_u}{R_y} \tag{20}$$

where, R_y = lateral deformation at yield and R_u = lateral deformation at ultimate.

Under lateral load, structure does not always show a well-defined yield point, therefore there are several ways to consider yield point for a structure under lateral load. Park (1988) summarized four commonly used ideas to define yield deformation of a structure in laboratory test. The idea of equivalent bilinear elasto-plastic yield point with reduced stiffness, as shown in Fig. 20**,** is recommended by Park (1988) since it considers deterioration of stiffness because of cracking and this stiffness deterioration is usual for real structure. Therefore, this idea is adopted in this study to define the experimental yield point (R_y) of the investigated test specimens at 75% of ultimate strength (i.e. $0.75Q_{max}$) as presented in Fig. 20. Most of the structures have some deformation capability beyond the peak resistance. Therefore, it is appropriate to consider the ultimate deformation capacity at the post-peak stage where load-carrying capacity reduces substantially (Park 1988). In this study, the ultimate deformation capacity (R_u) of the test specimen is considered at 20% lateral strength drop after peak resistance as shown in Fig. 20. All of the computed yield drifts and ultimate drifts are summarized in Table 5, which are further used to evaluate experimental ductility.

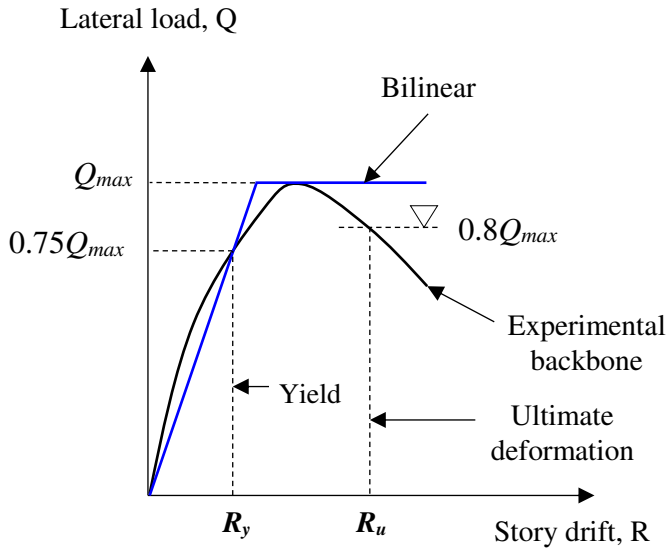

Fig. 20 Definition of yield and ultimate deformation of the test specimens

Table 5: Summary of the experimental yield (R_y), ultimate (R_{ult}) drifts and ductility factor (μ)

Specimen	Load transfer mechanism	Yield lateral drift, R_y	Ultimate lateral drift, $^*R_u$	Displacement ductility factor, $^*\mu_{exp}$
		%	%	
IM-FC-1	Mixed	0.10	0.55	5.50
IM-FC-2	Overall flexural	0.10	1.45	14.50
AR (Alwashali et al. 2020)	Column punching and joint sliding	0.56	1.88	3.36
IM-FC (Zahura et al. 2020)		0.21	0.83	3.95
Sp-5 (Kaya et al. 2018)	Diagonal compression	0.24	1.00	4.17
SMF (Demirel et al. 2015)		0.18	1.20	6.67
S5-FMFC (Seki et al. 2018)	Diagonal cracking and sliding	0.10	1.00	10.00
Sp-4 (Altin et al. 2010)		0.28	0.87	3.14
M3 (Zarnic and Tomazevic 1985)		0.34	2.00	5.88

* *Minimum of positive and negative loading is reported*

The experimental ductility factor (μ_{exp}) of all the investigated specimens are shown on normalized lateral load-displacement curve in Fig. 21. Overall flexural mechanism (Failure-I) exhibited a relatively high ductility (μ_{exp} =14) than other failure mechanisms. On the other hand, column punching and joint sliding failure (Failure II) showed relatively low ductility (μ_{exp} = 3.4 ~ 4), when compared to other failure mechanisms. Meanwhile, the diagonal compression mechanism (Failure-III) showed relatively higher ductility (μ_{exp} = 4.6 ~ 6.7) than the column punching-joint sliding mechanism (Failure-II), however less than diagonal cracking and flexural failure. Diagonal cracking and sliding mechanism (Failure-IV) showed ductility within a wide range of 3.4 ~10. The comparison of experimental ductility factors is also shown in Fig. 21, from which it is evident that overall flexural and diagonal cracking-sliding mechanism can be treated as ductile behavior. Whereas, column punching-joint sliding, and diagonal compression can be considered as a relatively brittle failure.

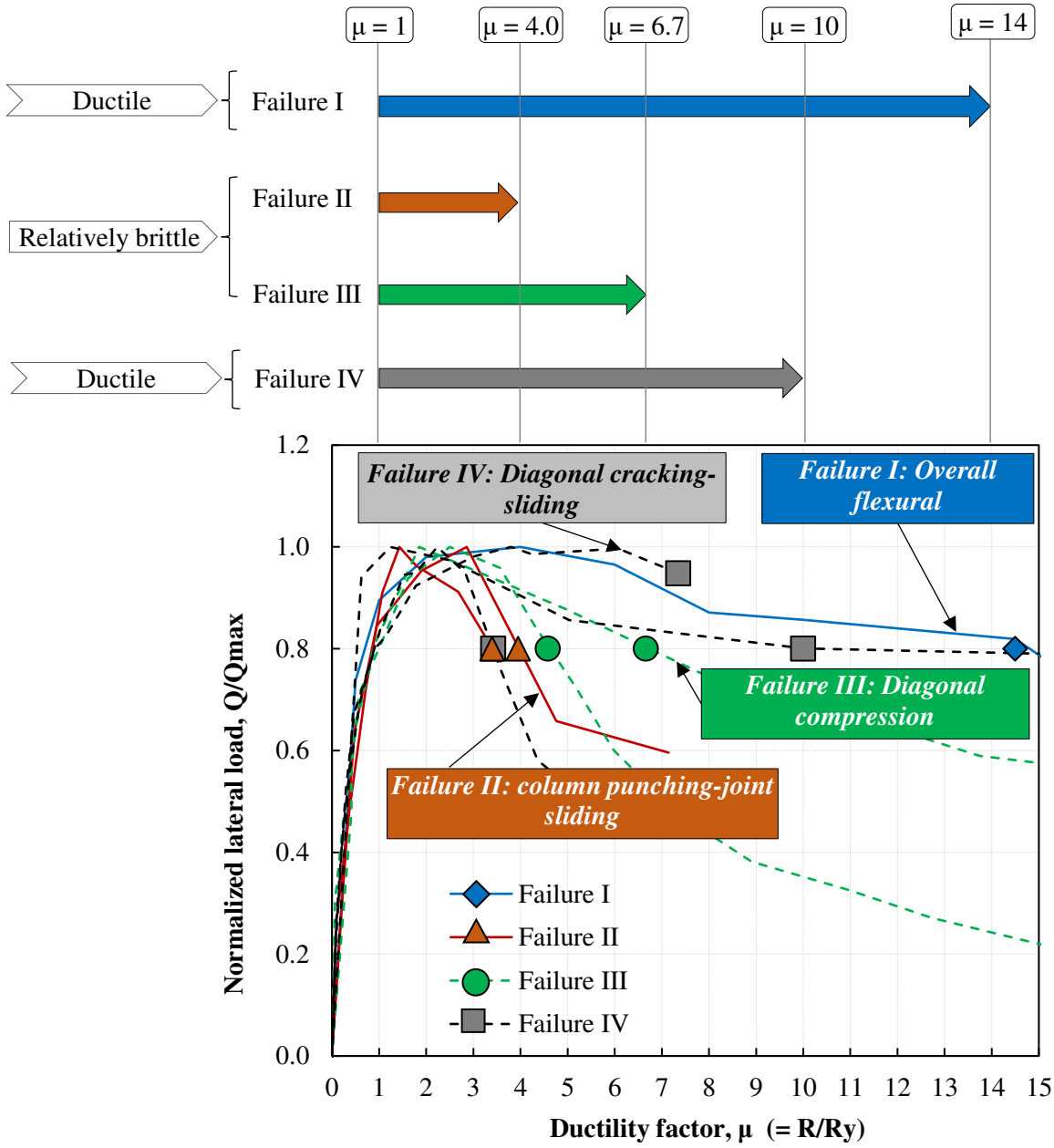

Fig. 21 Experimental ductility factor of all investigated test specimens

7 Conclusions

This study aims to identify and theoretically evaluate the major failure mechanisms of ferrocement strengthened masonry infilled RC frame through experimental endeavor. In addition, ductility of all identified failure mechanisms are also compared. Following conclusive remarks are drawn based on the scope of this study:

- Four distinct failure mechanisms i.e. load transfer mechanisms are recognized for ferrocement strengthened masonry infilled RC frame based on the experimental observation of this study, and past experimental investigations in literature. The failure mechanisms are as follows:
  - Failure I: Overall flexural

- Failure II: Column punching and joint sliding
- Failure III: Diagonal compression
- Failure IV: Diagonal cracking and sliding

o Theoretical lateral strength computation procedure is proposed for each failure mechanism which is followed by a proposal on lateral strength prediction and verification, with an average calculated to experimental lateral strength of 0.8 (CoV = 0.2).

o Overall flexural and diagonal cracking-sliding mechanisms exhibit relatively ductile behavior. Whereas, column punching-joint sliding, and diagonal compression mechanism can show a relatively brittle failure.

These conclusions are based on very limited number of test specimens; therefore, more studies are required before application of this evaluation procedure in real field.

References

ACI Committee 549R-97 (1997) State-of-the-Art report on ferrocement.

Adnan SMN, Fukutomi Y, Haga Y, Matsukawa K, and Nakano Y (2019) Experimental study of vulnerable rc frames with unreinforced masonry infill wall Part 1: Test program and results. Annual Meeting of the Architectural Institute of Japan 617–618.

Alcocer SM, and Flores L (2001) Tests on connectors for seismic retrofitting of concrete and masonry structures in Mexico. International RILEM Symposium on Connections between Steel and Concrete 481–490

Alcocer SM, Cesín JF, Flores LE, Hernández O, Meli R, and Tena A (2003) The New Mexico City building code requirements for design and construction of masonry structures. 9th North American Masonry Conference 656–667

Altin S, Anil Ö, Kopraman Y, Belgin Ç (2010) Strengthening masonry infill walls with reinforced plaster. Proceedings of the Institution of Civil Engineers: Structures and Buildings 163(5):331–42

Alwashali H, Sen D, Maeda M, Seki M (2020) Advantages and limitations of retrofitting masonry infilled RC frames by ferro-cement based on experimental observations advantages and limitations of retrofitting masonry infilled rc frames by ferro-cement based on experimental observations. 17th World Conference on Earthquake Engineering. Sendai, Japan.

Alwashali H, Torihata Y, Jin K, Maeda M (2018) Experimental observations on the in-plane behaviour of masonry wall infilled RC frames; focusing on deformation limits and backbone curve. Bulletin of Earthquake Engineering 16(3):1373–97.

Anderson DL, Priestley MJN (1992) In plane shear strength of masonry walls. 6th Canadian masonry symposium 223–234

ASCE/SEI 41-06 (2007) Seismic rehabilitation of existing buildings.

ASTM (2011) ASTM C 1314–03b: Standard test method for compressive strength of masonry prisms.

Canadian Standards Association (2004) CSA S304.1-04 Design of masonry structures

Crisafulli FJ (1997) Seismic behaviour of reinforced concrete structures with masonry infills. Dissertation, University of Canterbury

Demirel IO, Yakut A, Binici B, Canbay E (2015) An experimental investigation of infill behaviour in RC frames. 10th Pacific Conference on Earthquake Engineering 1–8

FEMA 306 (1998) Evaluation of earthquake damaged concrete and masonry wall buildings

Hetenyi M (1946) Beams on elastic foundation theory with applications in the fields of civil and mechanical engineering. Michigan, USA: The university of Michigan Press.

Japan Building Disaster Prevention Association (JBDPA) (2001) Standard for seismic evaluation of existing reinforced concrete buildings.

Japanese Industrial Standards (2010) No. JIS R1250, JIS Z 2201, JIS A 1108, JIS A 1113 [in Japanese]

Kaya F, Tekeli H, Anil Ö (2018) Experimental behavior of strengthening of masonry infilled reinforced concrete frames by adding rebar-reinforced stucco. Structural Concrete 19(6):1792–1805

Mander JB and Nair B (1994) Seismic resistance of brick-infilled steel frames with and without retrofit. The Masonry Journal 12(2):24–37

MSJC (2011) Building Code Requirements and Specification for Masonry Structures: Containing Building Code Requirements for Masonry Structures (TMS 402-11/ACI 530-11/ASCE 5-11) [and] Specification for Masonry Structures (TMS 602-11/ACI 530.1-11/ASCE 6-11) and Companio.

Naaman AE (2000) Ferrocement and laminated cementitious composites. Michigan, USA: Techno Press

New Zealand Standard (2004) NZS 4230 Design of reinforced concrete masonry structures.

Park R (1988) State-of-the Art Report: ductility evaluation from laboratory and analytical testing. 9th World Conference on Earthquake Engineering 605–616

Seki M, Popa V, Lozinca E, Dutu A, Papurcu A (2018) Experimental study on retrofit technologies for RC frames with infilled brick masonry walls in developing countries. 16th ECEE 1–12

Sen D (2020) Identification of failure mechanism and seismic performance evaluation of masonry infilled RC frame strengthened by ferrocement. Dissertation, Tohoku University

Sen D, Alwashali H, Islam MS, Maeda M (2020) Investigation of the lateral capacity of ferro-cement investigation of the lateral retrofitted masonry capacity masonry in RC frame and simplified prediction approach. AIJ Journal of Technology and Design 26(62):159–63

Smith BS (1966) Behavior of square infilled frames. Journal of the Structural Division 92(1): 381–404.

Yamamoto Y (1990) Ultimate shear strength of reinforced concrete members with extremely small shear span ratios. Workshop on Evaluation, Repair, and Retrofit of Structures — U.S.-Japan Panel on Wind and Seismic Effects. Gaithersburg 3-6-1-3-6–13

Zahura F, Sen D, Sabrin R, Das A, Uddin MJ, Tafheem Z, Khanam F, Alwashali H, Maeda M (2020) In-Plane seismic performance of masonry infilled RC frame with and without ferrocement overlay. 17th World Conference on Earthquake Engineering, Sendai, Japan.

Zarnic R, Tomazevic M (1985) Study of the behaviour of masonry infilled reinforced concrete frames subjected to seismic loading. 7th International Conference on Brick Masonry Australia 1315–1326

Figures

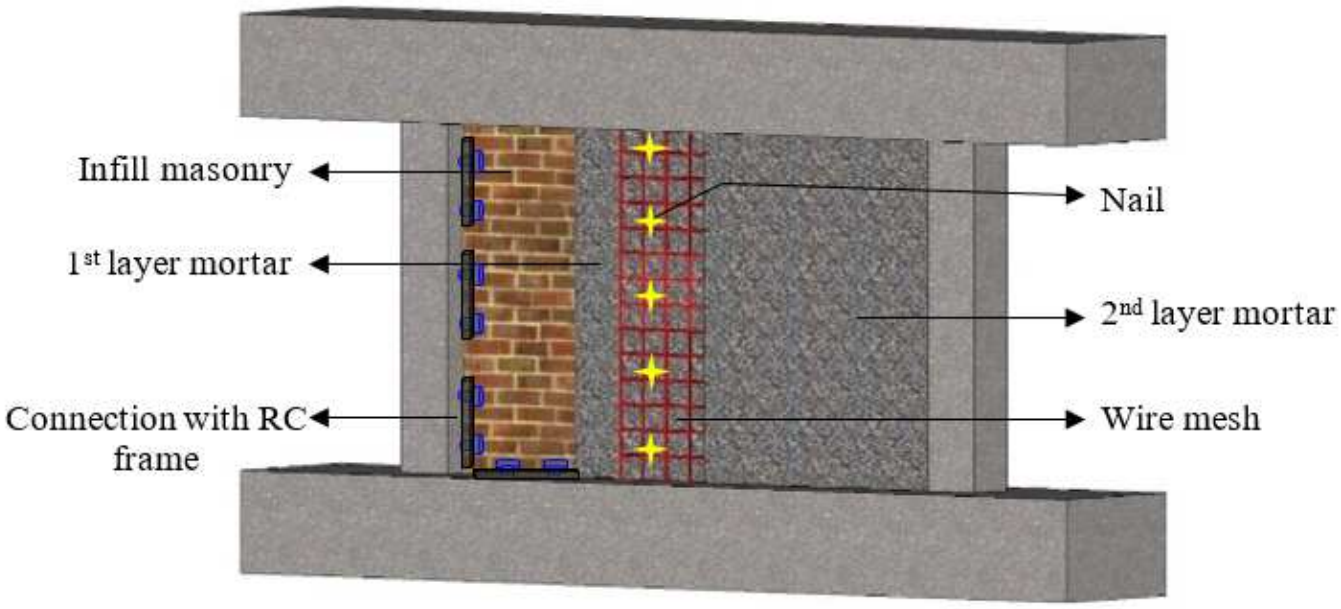

Figure 1

Schematic diagram of FC strengthened masonry infill

Figure 2

Extremely short column i.e. punching failure of tension column (Crisafulli 1997)

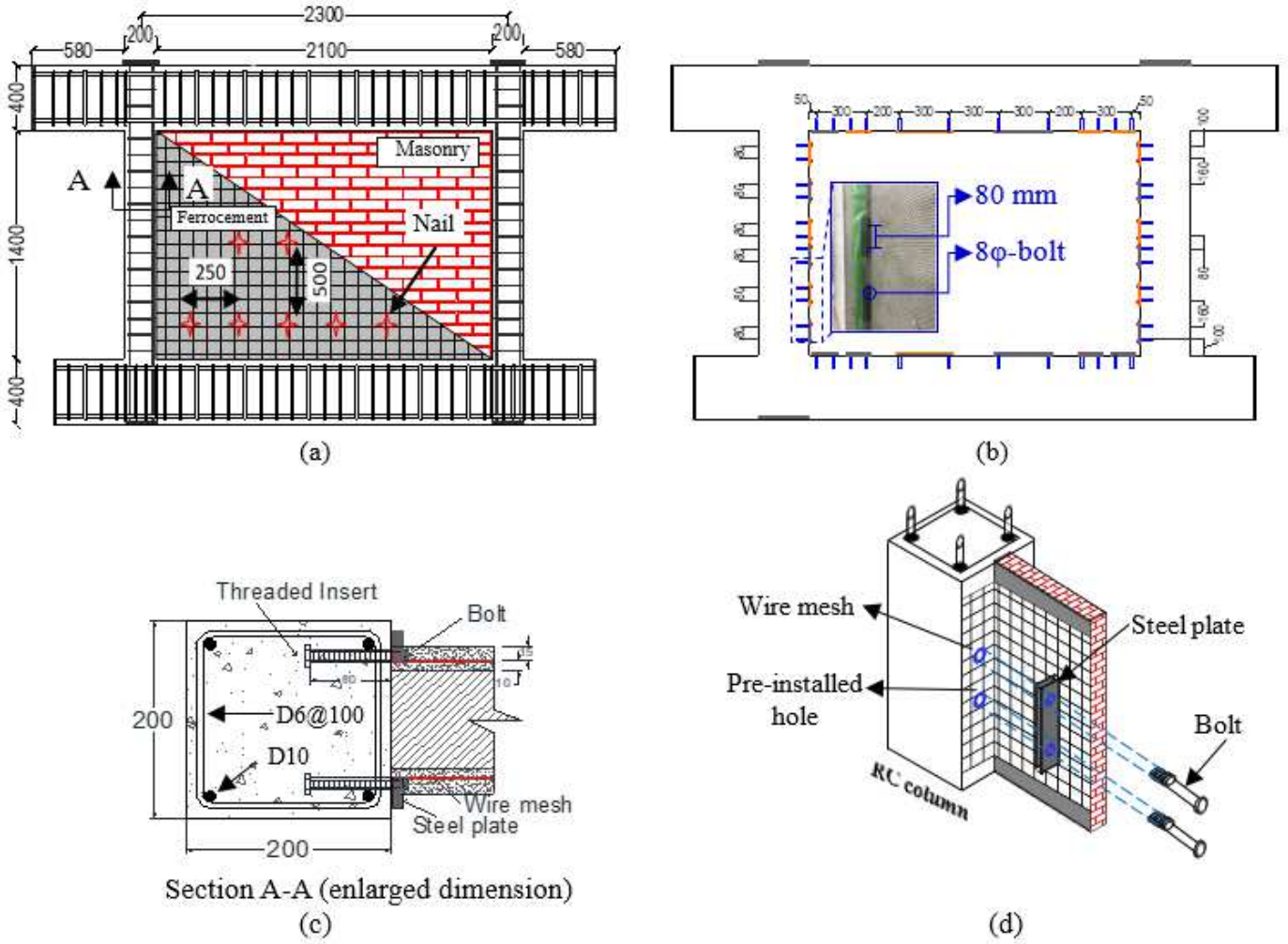

Figure 3

(a) geometry of test specimen (dimension in mm) (b) locations of drilled holes in RC frame and (c) cross section of column and (d) connection method of wire mesh with RC frame (both columns and beams)

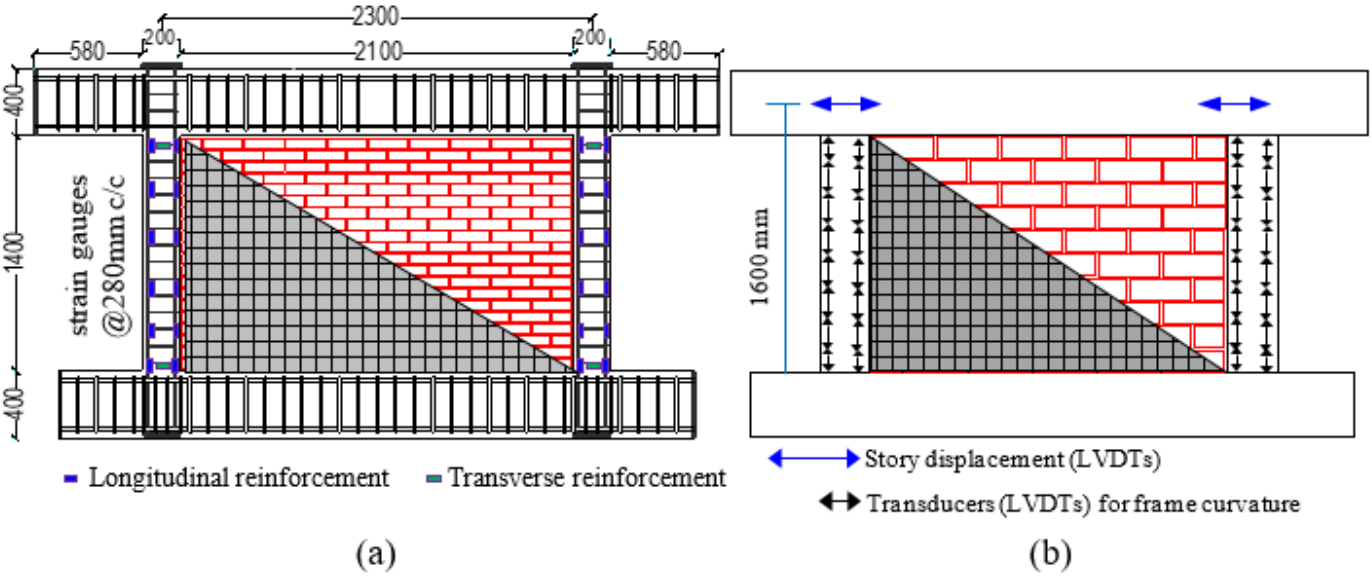

Figure 4

Location of (a) strain gauges and (b) transducers on columns

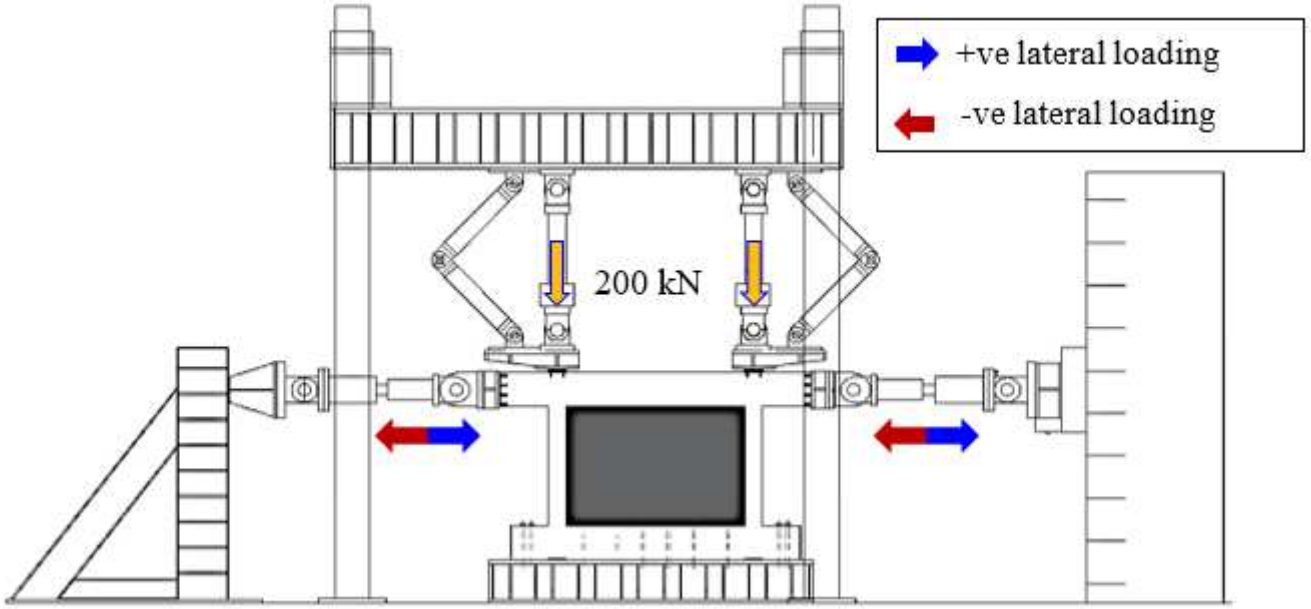

Figure 5

Test specimen loading system

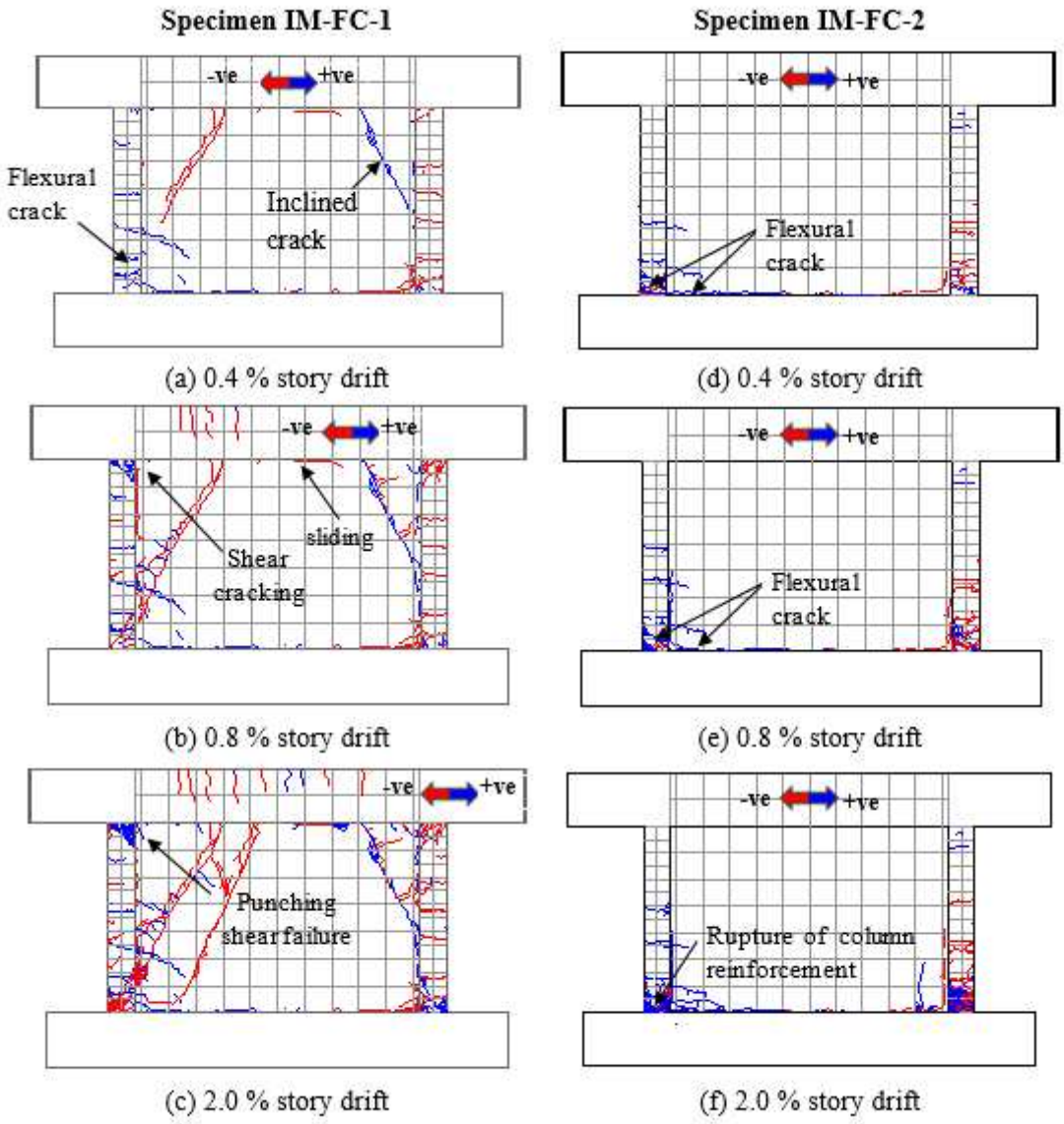

Figure 6

Crack propagation of specimens (IM-FC-1 and IM-FC-2)

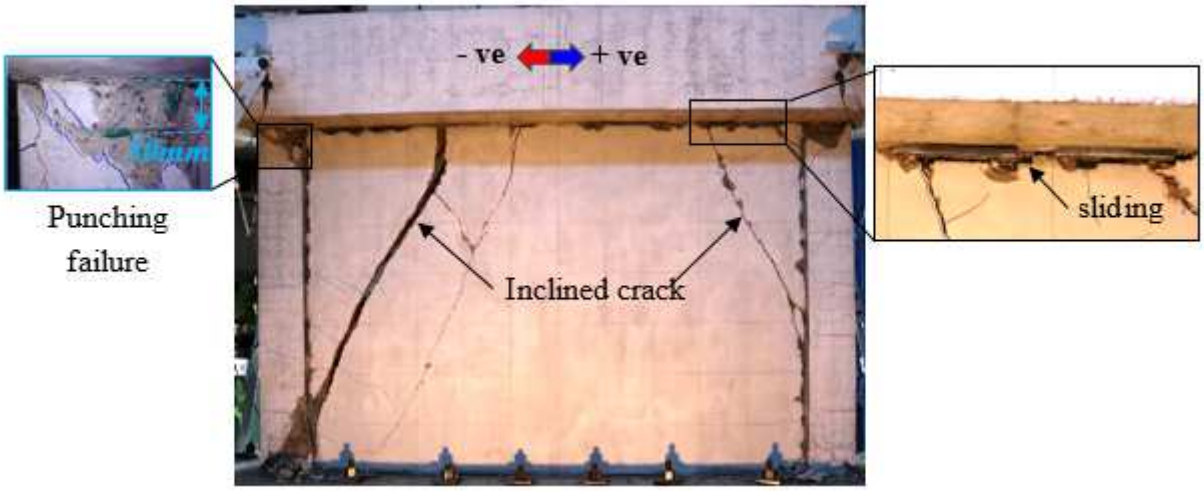

Figure 7

Final damage state of specimen IM-FC-1

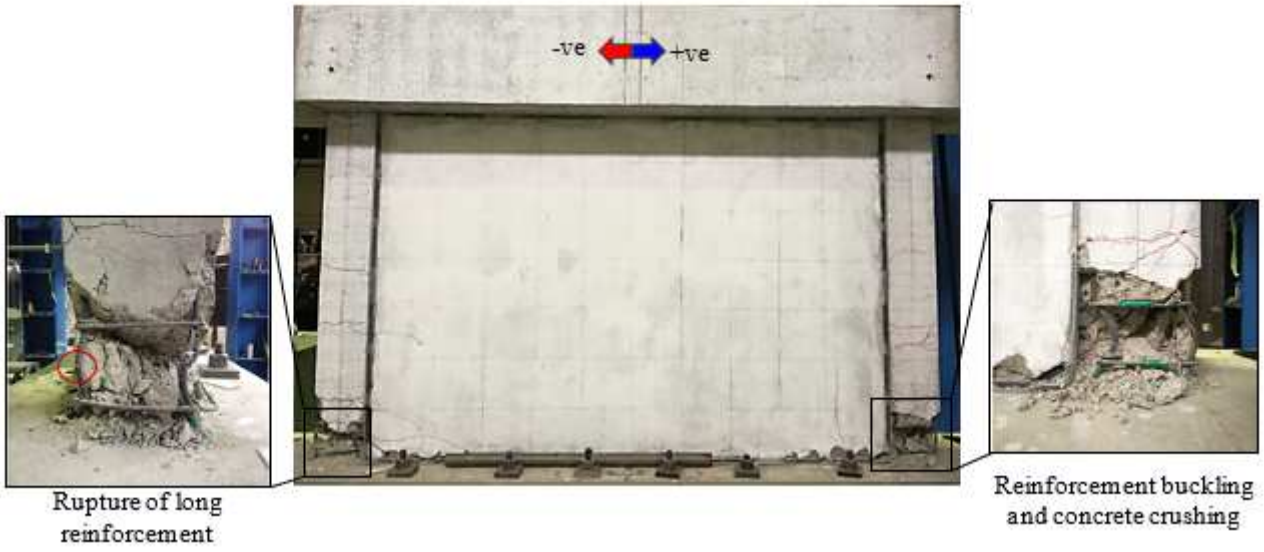

Figure 8

Final damage state of specimen IM-FC-2

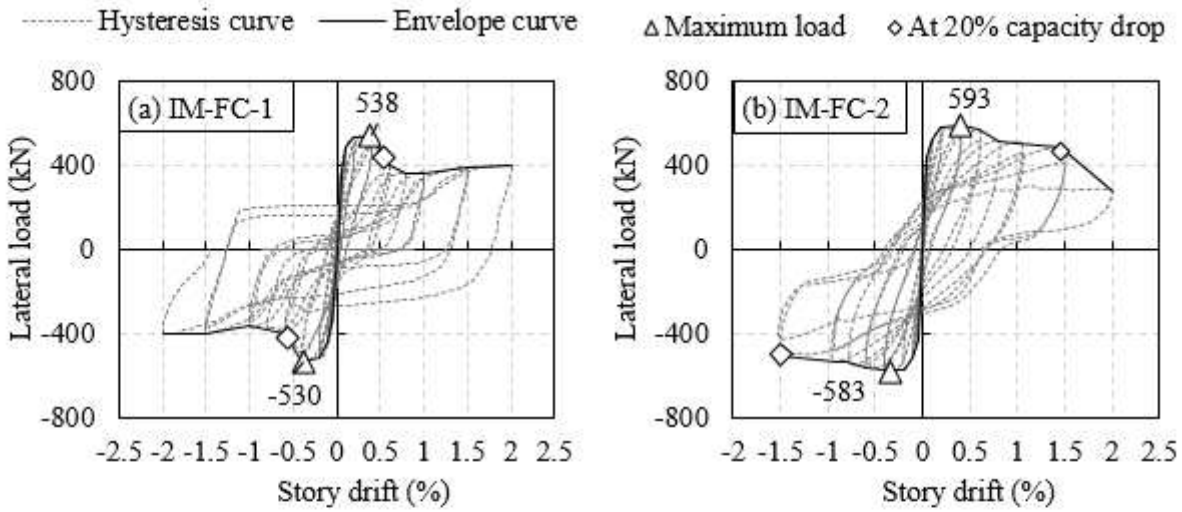

Major incidents (IM-FC-1)

0.1~0.2%: *main bars in tension columns yielded*
0.4%: *peak load resistance and inclined crack on wall*
0.6%: *shear crack at tension column's top and sliding started at top of wall*
1.5%: *punching shear failure at tension column top*

Major incidents (IM-FC-2)

0.1%: *main bars in tension columns yielded*
0.4%: *peak load resistance*
1.5%: *wire mesh at bottom of tension side ruptured and compression column bottom concrete crushed*
2%: *three out of four main reinforcements of tension column ruptured*

Figure 9

Lateral load-story drift relationship of specimen IM-FC-1 and IM-FC-2

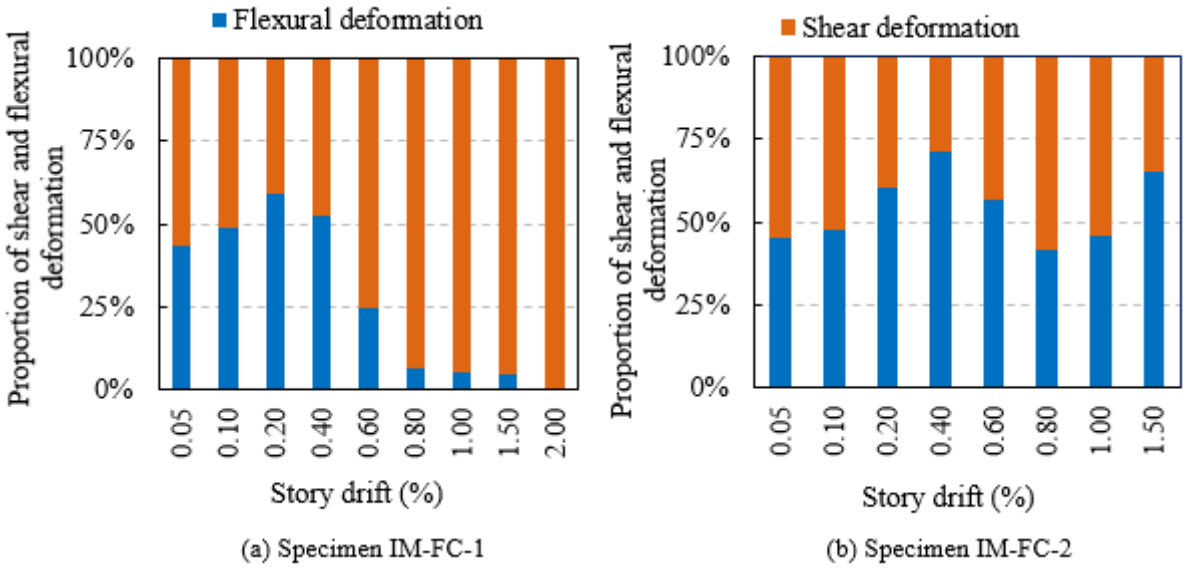

Figure 10

Flexural and shear components of story deformation of specimen IM-FC-1 and IM-FC-2

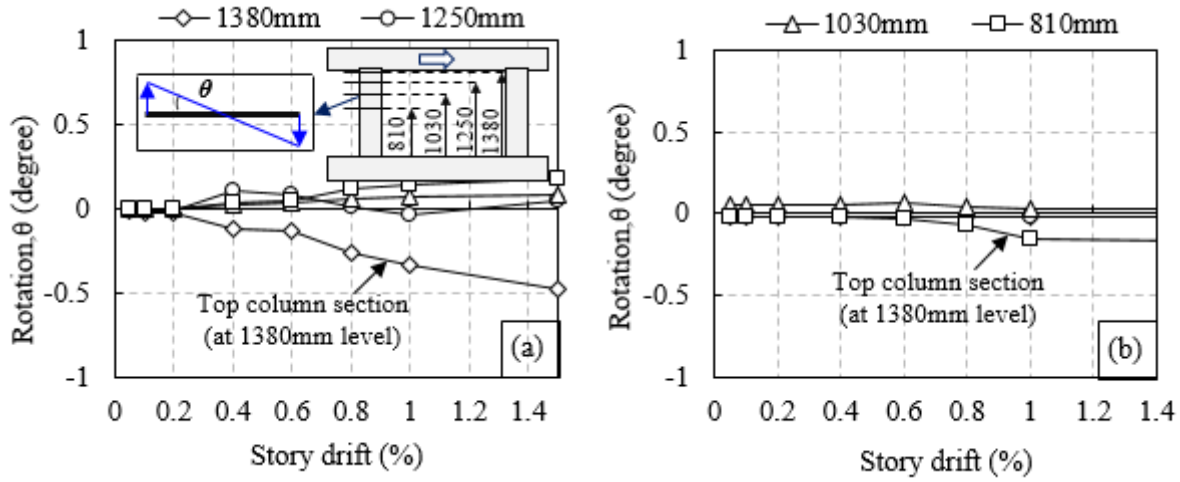

Figure 11

Rotation of tension column at several sections of specimen IM-FC-1 and IM-FC-2

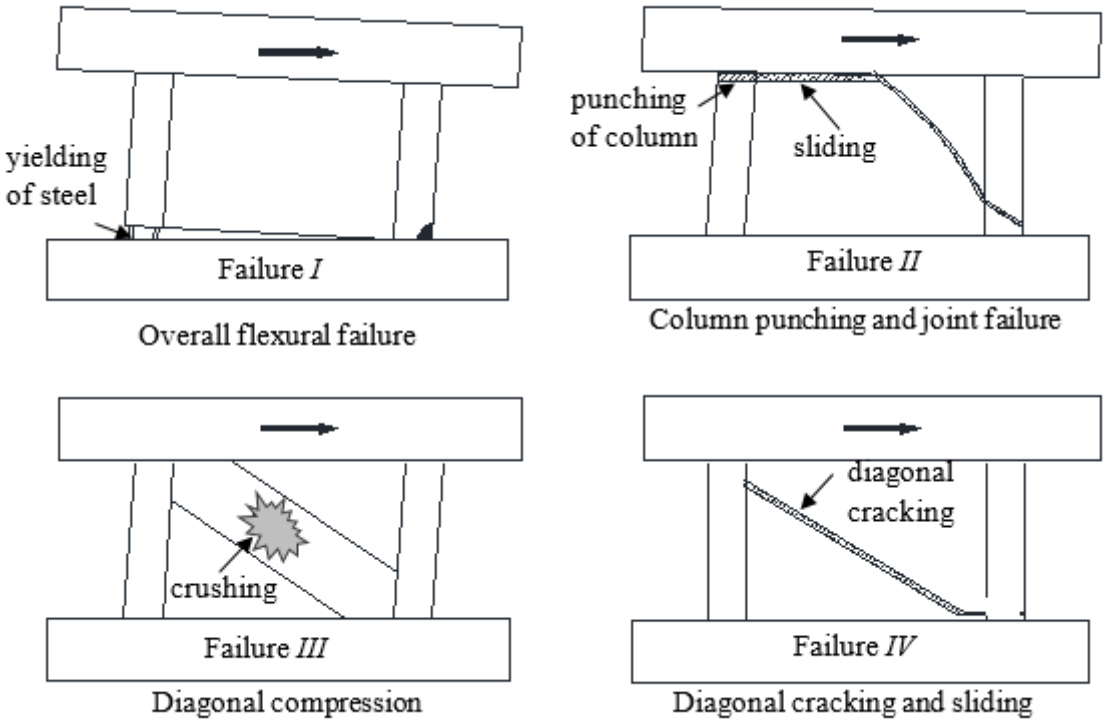

Figure 12

Major failure mechanisms of FC strengthened masonry infilled RC frame

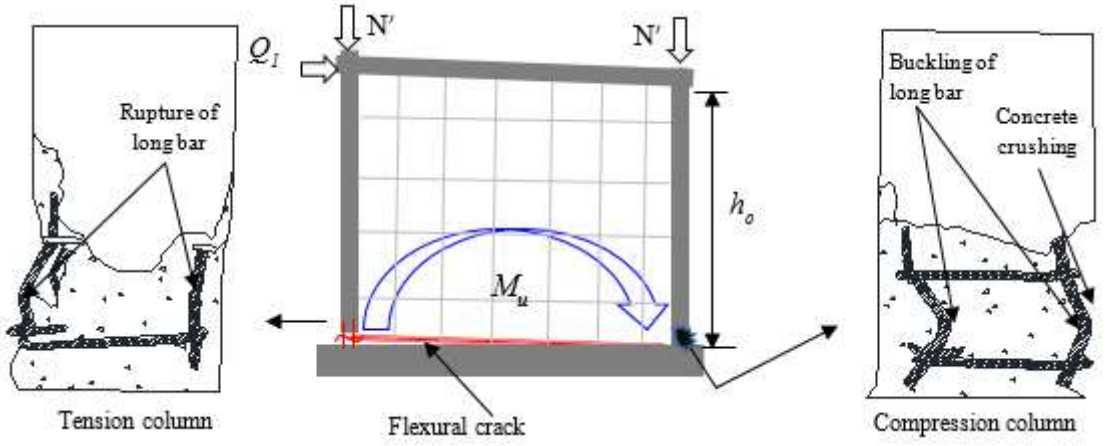

Figure 13

Load transfer mechanism of overall flexural failure (Failure I)

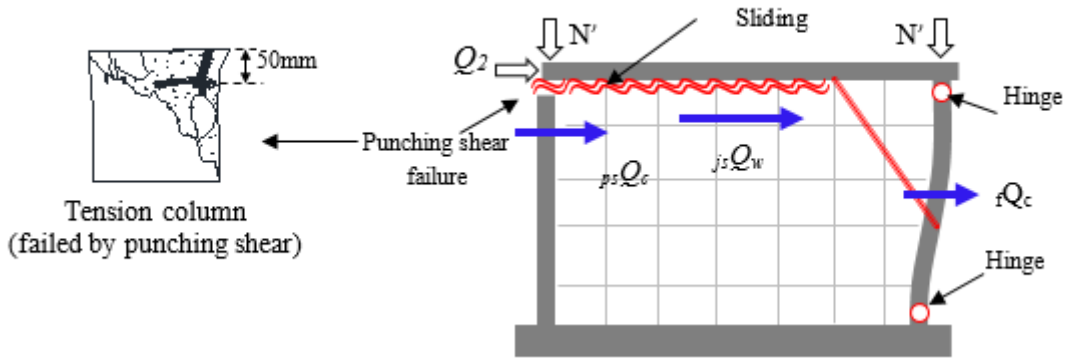

Figure 14

Idealized load transfer mechanism of column punching and joint failure (Failure II)

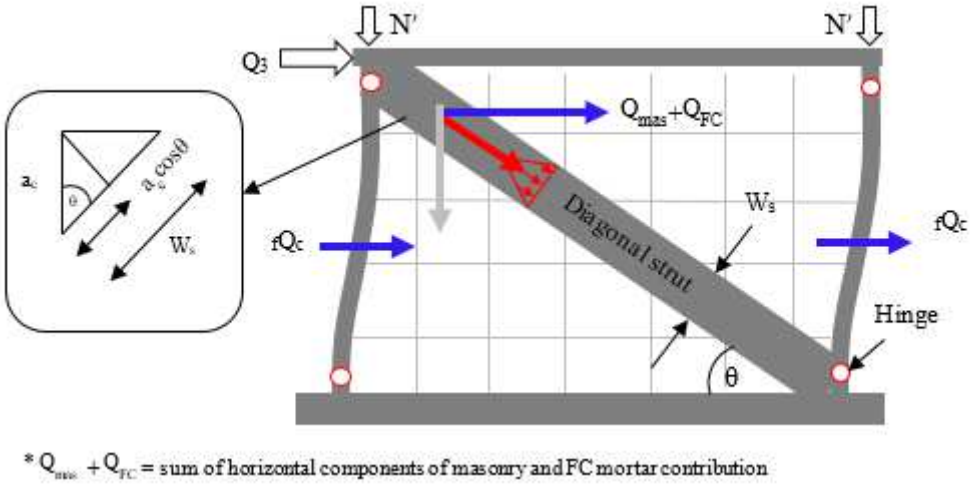

Figure 15

Idealized load transfer mechanism of diagonal compression failure (Failure III)

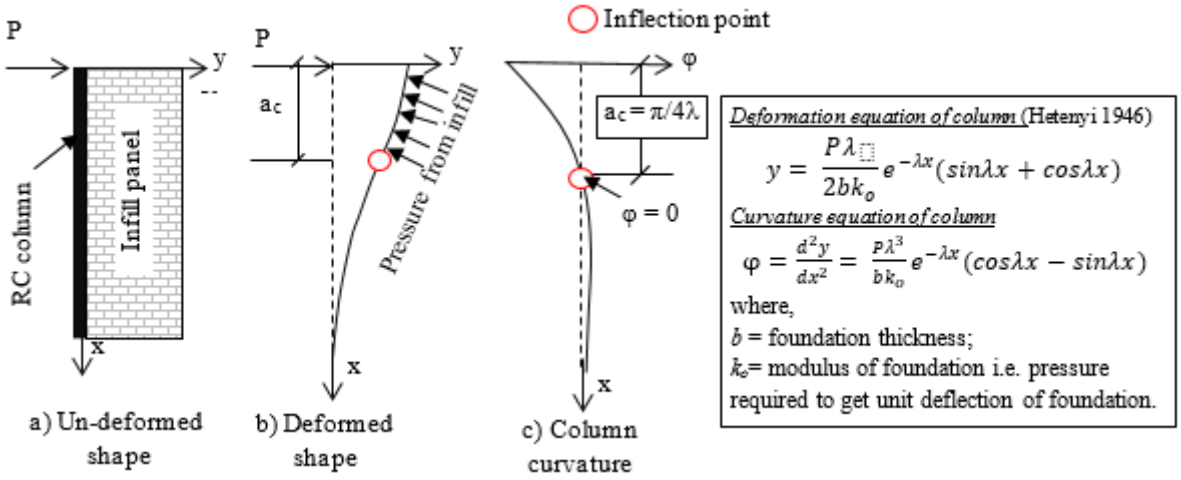

Figure 16

Surrounding RC column (a) un-deformed shape, (b) deformed shape and (c) curvature distribution

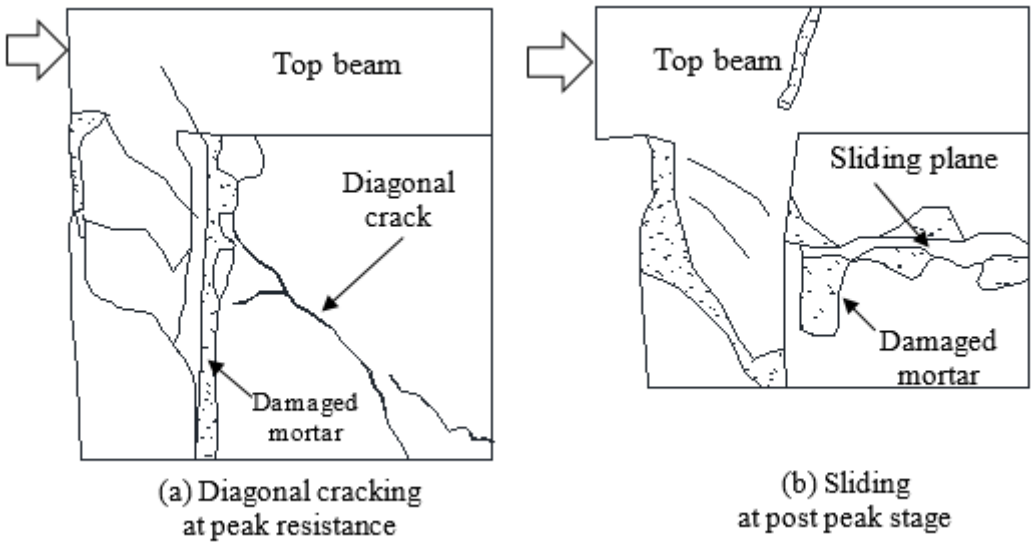

Figure 17

Damage (a) at peak resistance (back view) and (b) at post peak stage (front view) of specimen S5-FMFC (Seki et al. 2018)

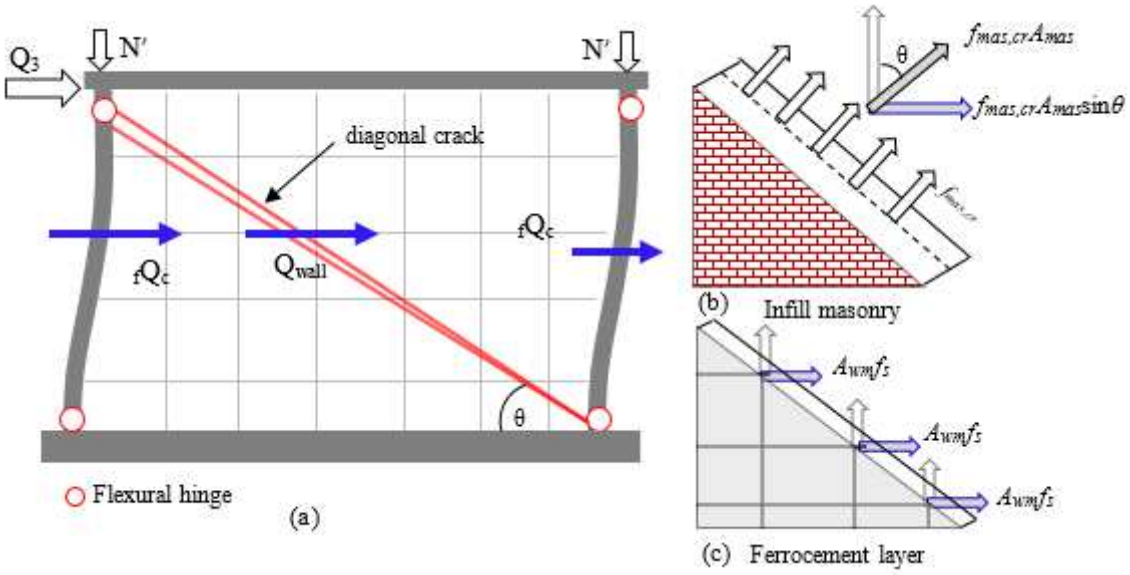

Figure 18

(a) Idealized load transfer mechanism of diagonal cracking and sliding (Failure IV) (b) cracked infill masonry and (c) cracked ferrocement layer

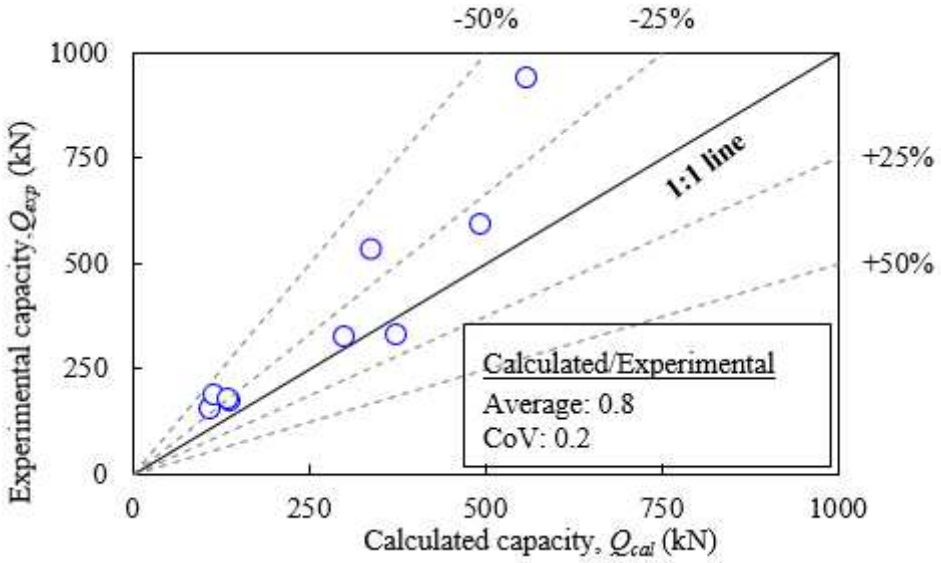

Figure 19

Calculated and experimental capacities all investigated specimens

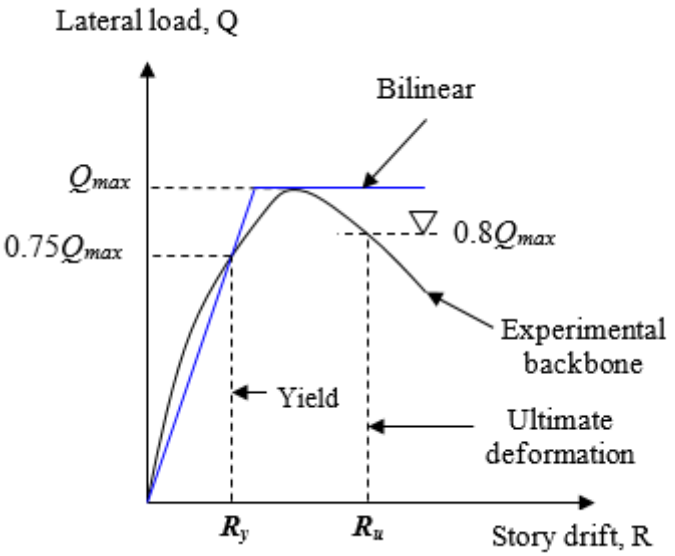

Figure 20

Definition of yield and ultimate deformation of the test specimens

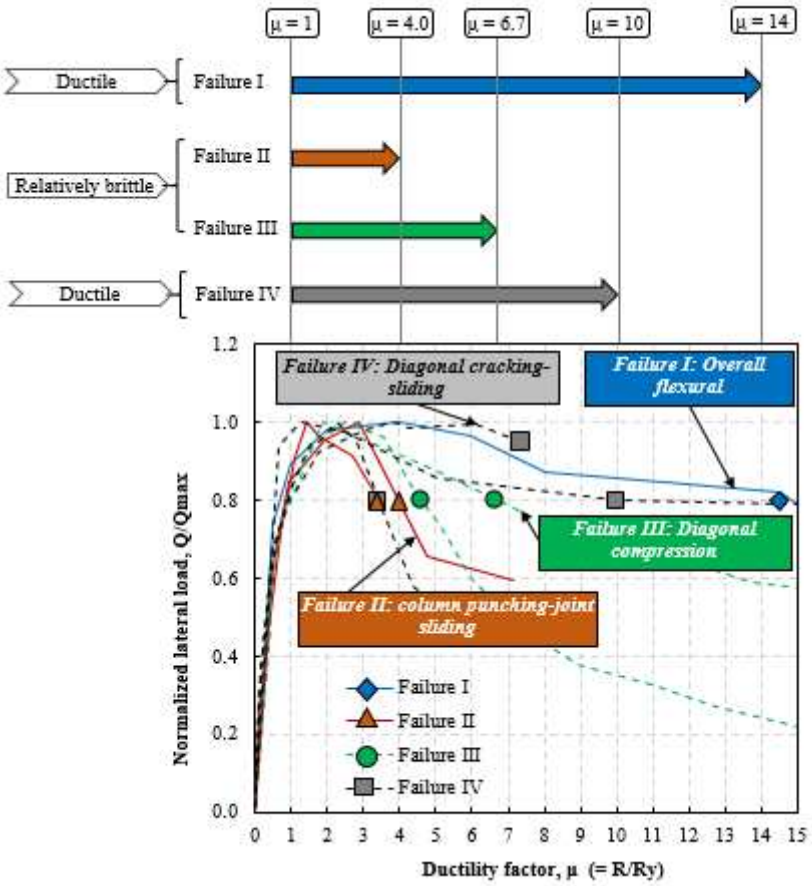

Figure 21

Experimental ductility factor of all investigated test specimens